12-2005

Design of a Novel Reluctance Motor for Industrial Applications

Weston Clute Johnson
University of Tennessee - Knoxville

To the Graduate Council:

I am submitting herewith a thesis written by Weston Clute Johnson entitled "Design of a Novel Reluctance Motor for Industrial Applications." I have examined the final electronic copy of this thesis for form and content and recommend that it be accepted in partial fulfillment of the requirements for the degree of Master of Science, with a major in Electrical Engineering.

John Chiasson, Major Professor

We have read this thesis and recommend its acceptance:

Leon Tolbert, Jack Lawler

Accepted for the Council:
Carolyn R. Hodges

Vice Provost and Dean of the Graduate School

(Original signatures are on file with official student records.)

To the Graduate Council:

I am submitting herewith a thesis written by Weston Clute Johnson entitled "Design of a Novel Reluctance Motor for Industrial Applications". I have examined the final electronic copy of this thesis for form and content and recommend that it be accepted in partial fulfillment of the requirments for the degree of Masters of Science with a major in Electrical Engineering.

John Chiasson

Major Professor

We have read this thesis
and recommend its acceptance:

Leon Tolbert

Jack Lawler

Acceptance for the Council:

Anne Meyhew

Vice Provost and Dean of Graduate Studies

(Original signatures are on file with official student records.)

Design of a Novel Reluctance Motor for Industrial Applications

A Thesis
Presented for the
Masters of Science
Degree
The University of Tennessee, Knoxville

Weston Clute Johnson
December, 2005

Abstract

A novel reluctance motor topology, termed the Johnson-Currie Reluctance Motor (JCRM), has been developed and described in this thesis. The JCRM topology and analysis is based upon the traditional switched reluctance motor (SRM) topology although there are significant modifications.

The flux path of the JCRM topology is such that it passes through the rotor and stator in three-dimensions. This topology with three dimensional flux paths allows for the removal of discrete stator windings giving rise to vastly superior maintance to the traditional SRM and arguably to most electric motors. In addition, the usage of three-dimensions for flux paths gives rise to increased energy density compared to other motor topologies, SRM or otherwise.

However, the new topology also gives rise to increased complexity in design and control. The topology creates a host of new motor constraints that must all be optimized for successful design.

Contents

List of Figures

Chapter 1

Introduction

This thesis thoroughly describes the analysis of a new reluctance based motor topology. The topology of this new motor is shown to have characteristics of a traditional switched reluctance motor (SRM) as well as those of the induction motor. The new topology is shown to have the low cost typically associated with SRMs, all while significantly improving upon maintenance that traditional machines lack. It is the intention to prove that this new topology will fulfill the needs of industry for existing and future applications.

This new motor has been designed, with the sole purpose of proving the concept of the novel topology. As the overall purpose is to prove the concept and obtain a baseline model, some design simplifications have been made to help ease the analysis. Each design simplification shall be explained as encountered.

Chapter 2 begins with a global perspective of why a new more efficient and higher

performance motor is needed. This "big picture" includes a review of existing motor applications and their inadequate nature for meeting the long term goals. Chapter 2 explains that this inadequacy lies primarily in the fact that existing motors, SRM, induction or otherwise, typically have a relatively high base speed whereas many applications require low speed and high torque. This uneven match is balanced through the use of speed reducers (gears), which add cost and decrease system efficiency. Chapter 2 continues with a description of traditional SRM designs and the basis for their analysis.

Chapter 3 begins with a thorough description of the new topology, starting with a detailed explanation of each piece of the new motor. The motor fundamentals are then shown to have several variations that may be configured for specific applications adding to the uniqueness and advantage of the new topology. Based upon the description of the motor topology, it is hoped that the reader should recognize that while the proposed topology is not an intuitive first design, one would wonder why this topology has not been done previously. The chapter continues with an explanation of flux transitions and flux rotation, a fundamental difference between the new topology and traditional designs.

Chapter 4 describes the analysis of the motor, based upon techniques used for the traditional SRM.

Chapter 5 gives simulation results and a comparison between the JCRM and a traditional SRM design. The simulations show that the JCRM needs further refine-

ment prior to fabrication and yet stand as evidence that the concept is valid and of benefit.

Chapter 6 completes this thesis with final results and conclusions from the design, analysis and modeling of the motor. Chapter 6 is completed with a listing of future work to further extend the proposed motors performance and industrial acceptance.

Chapter 2

Background

In 2003, roughly 7.5 billion dollars of motors and generators were shipped in the US [1]. Electric motors account for about 64% of all consumed electricity in the industrial sector, roughly 290 billion kwh per year [1]. Of these motors, over 95% are fractional horsepower (<746W) [1]. With this in mind, and the numerous environmental quality issues that are ever present, it becomes clear that improving the efficiency of electric motors, specifically within the industrial markets, will have the greatest effect in solving global environmental issues without severe disruption to the global economy. For these reasons, i.e. environmental and economic, the electric motor as a source of rotational power, will be re-examined.

The most common application of an electric motor is as a constant speed, variable torque power source. The typical application includes pumps, fans, conveyors, and machining equipment. To fulfill such application requirements, an induction motor

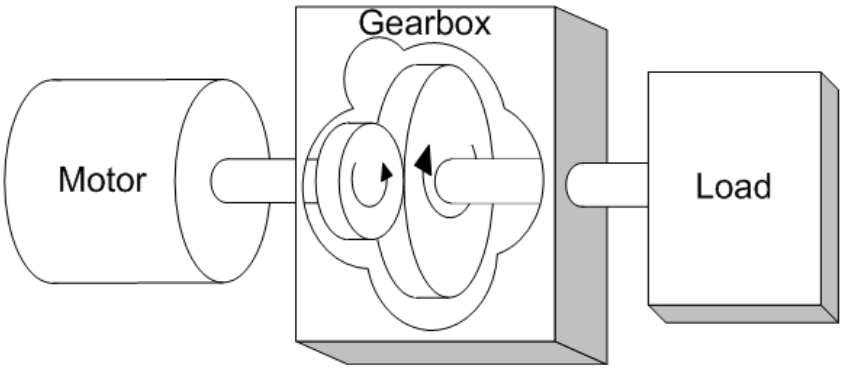

Figure 2.1: Typical Motor and Gear Combination

with little more than a motor starter (contacts and overload protection) for control and simple gear reducer (gearbox) for producing the desired speed are required. Typical induction motors have a rated speed of about 1800 RPM depending upon the pole count, supply frequency, etc. While this speed is ideally suited for a few applications, most applications require a much lower speed. Pumps, fans, conveyors, and so on, typically operate at only a few hundred RPM as otherwise they risk damage to their load or product. For this reason, excess motor speed is converted, via a gearbox, to a lower speed and a higher torque. Figure 2.1 shows this typical relationship between a motor, gearbox and load. In these applications, the employment of simple controls (motor starter) and a single gear reducer is no longer sufficient. This is because these applications typically require multiple reducers as a single gear reducer cannot reduce the developed motor speed to the desired speed and torque as the space requirements would be extreme.

Applications which require high torque include rock crushing, marine vessel propulsion, mining, and some traction drive applications. Due to this inability to develop the desired speed and torque directly from the motor, inefficiency is introduced into the overall system by the requirement of a gearbox. This inefficiency arises from the transformation of the input energy. In every energy transformation, from electrical to mechanical and/or mechanical-to-mechanical, losses are occurring and they occur in a compounding manner. For instance, a motor with an assumed efficiency of 95% and a gearbox with two reductions with efficiency of 97% each, results in an overall system efficiency of 89% ($0.95 * 0.97 * 0.97 = 0.89$). This means an 11% higher electrical cost for the equipment user as well as increased environmental impact from the electrical power supplier. Despite these high losses, this scenario has been accepted as "the way things are done" since the age of steam power.

Ideally, these large torque applications could be solved with a direct drive motor, one in which there were no gearboxes or other speed reducers. For this to occur, the exact speed and torque, to perfectly meet the specific application requirements, would have to be produced in a single operation thus removing all associated inefficiencies due to unnecessary energy transfers associated with the traditional motor/gear combination.

Traditionally, few options exist for high torque industrial applications. The motor topologies considered viable for these applications are the induction motor (IM), permanent-magnet motor (PMM) and the switched reluctance motor (SRM) which

has only become viable in the last two decades due to advances in power electronics. Despite this late coming, the SRM is able to perform in a roughly equivalent manner to the IM and PMM when properly designed. While the performances are roughly equal, IMs have a vast knowledge base and infrastructure and are thus the most prevalent type of industrial motor because the technology for the other types was previously inadequate or the cost too great. Despite the IM popularity, PMM and SRM topologies are generally considered superior machines as they have higher efficiencies and higher specific power than the IM. From an economic perspective, especially for large applications, the cost of the permanent-magnet for the PMM will be greater than the IM or SRM due their magnets, thus typically eliminating the PMM topology as a viable candidate for large industrial application. Again, from an economic view point, the SRM will typically have a lower manufacturing cost than a single speed induction motor without a controller thus making it a clear choice for industrial application. The reasons for this lower cost include simpler rotor design and simpler coil-windings. Despite this clear choice for the SRM topology, the topology has been under-utilized in industry for various reasons, including torque ripple, windage, and a previous lack of hardware and techniques to control this highly non-linear machine.

2.1 SRM Topology

The traditional SRM topology is doubly salient, meaning that the stator and rotor are composed of *salient poles.* The stator poles are arranged and combined such that they envelop the rotor which is also composed of salient poles whose number of poles does not equal the stator's. Wrapped around the stator's salient poles are the motors windings. (The SRM topology does not have rotor windings.)

The term *switched reluctance motor* is perhaps misleading. While the reluctance is switched, it is done so as the by-product of current switching or commutation from one phase to another. *Reluctance* actually describes a material's ability to conduct a magnetic field as described in Equation 2.1.

$$\Re = \frac{l}{\mu A} \tag{2.1}$$

The reluctance $\Re$ accounts for material and geometric properties of the motor where l is the path length of the flux, μ is the permeability of the material and A is the cross-sectional area of the path length. Typically, electric motors are described with by their input electrical properties because these parameters are adjustable, during operation of the motor. However, in designing the physical motor, these electrical properties are resultants of the physical motor design.

As current in the windings is increased, a magnetic field will develop between the stator and rotor, developing a torque, resulting in the rotor's motion. Torque production is made in a plane(s) perpendicular to the axis of the shaft and a plane(s) parallel to the plane of rotation, as shown in Figure 2.2, and thus can be thought of

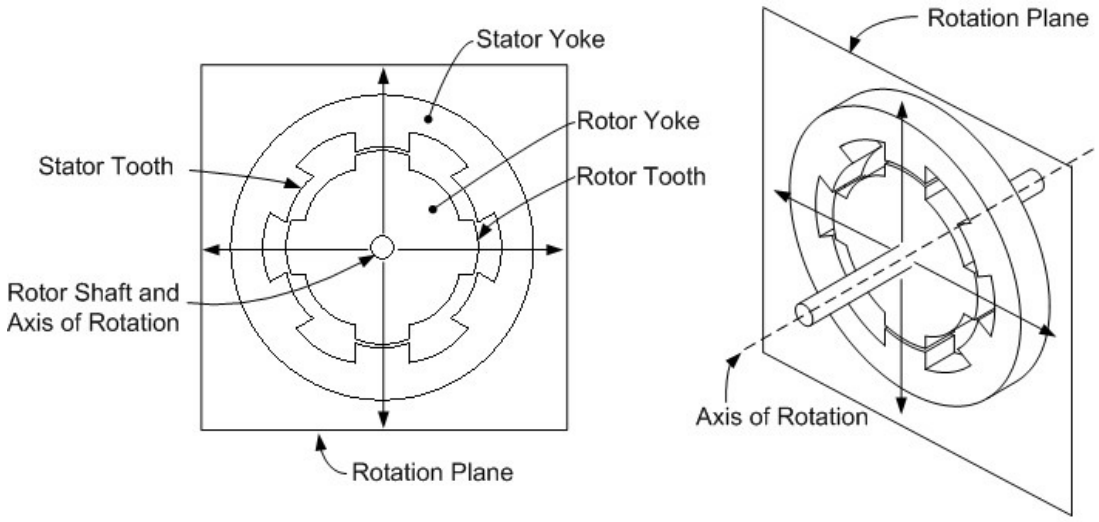

Figure 2.2: Traditional S6/R4 SRM Topology

as being developed in a two-dimensional plane.

The rotor will tend to rotate such that the reluctance of the flux path is minimized. As the rotor approaches alignment with the initiating pole, torque generation drops as the flux linkage approaches its maximum value. As alignment occurs, commutation with a different rotor pole is initiated thus repeating the process.

As current is introduced into a stator phase winding of an SRM, flux along the path of minimum reluctance will develop. Because the minimum reluctance is dependant upon rotor position, the resulting flux linkage in the winding is thus a function of current and rotor position. By design, this path of minimum reluctance between the stator and rotor primarily traverses the stator pole through the air gap, through the rotor tooth, then through the rotor yoke, then through the opposite side rotor tooth, then through the opposite side air gap, before re-entering the stator yoke through the

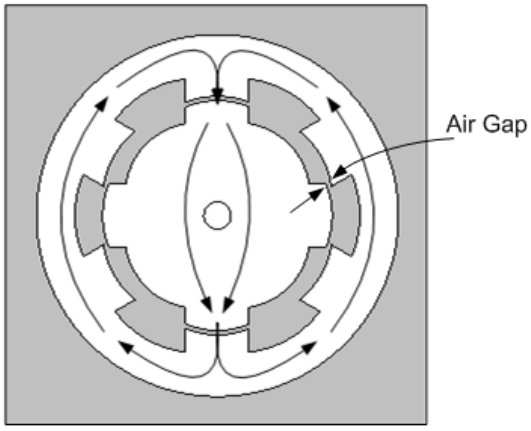

Figure 2.3: Flux Path of Traditional S6/R4 SRM

opposite side stator tooth to return to the initial stator tooth and thus completing the magnetic circuit. This magnetic path is shown in Figure 2.3.

Figure 2.3 shows the flux path for an S6/R4 SRM. The notation S6 indicates a stator yoke with six teeth and a notation of R4 denotes a rotor yoke with four teeth. This is a typical SRM design although there are many variations to this SRM topology. Variations to this design include a multitude of teeth configurations on both the rotor and stator as well as various pole configurations from single pole to multiple (>10 in some cases) depending upon the application and desired results [3]. Independent of the pole count, or tooth design, flux linkage and thus torque, is still primarily established in a plane or planes perpendicular to the axis of rotation as shown in Figure 2.2.

Notice also that for the S6/R4 configuration, only two rotor teeth are being utilized during each step of the rotor. This point is addressed further in the next chapter.

2.2 SRM Analysis

The analysis of the SRM is done from a conservation of energy approach and is typically analyzed as a single phase motor because the flux linkages and resulting mutual inductance between phases is typically negligible. In addition, the motor is assumed to be perfectly symmetric between each phase. To obtain the characteristics for the entire motor all phases must be included and is done so by adding the proper phase offsets as necessary.

The flux linkage, is given in Equation 2.2.

$$\Psi = N\Phi = \frac{N^2}{\Re} i = \int_0^t e_a(t)dt = \int_0^t (V_S - Ri)dt = \frac{1}{\omega}\int_{\theta_0}^{\theta} (V_S - Ri)d\theta \qquad (2.2)$$

As seen in Equation 2.2, flux linkage is given in both magnetic and electrical terms where flux linkage is Ψ, the number of coil windings in a phase is N, the flux is Φ, i is the current, e_a is the phase voltage, V_S is the supply voltage, and ω is the speed. The SRM is generally characterized by this equation which results in a plot of flux linkage versus current shown in Figure 2.4.

Figure 2.4 shows a typical magnetization curve for a fixed rotor position. The area above the magnetization curve is the field energy (W_E), produced by the stator windings. The area below the curve given by $W_C = \int_0^i \Psi(\theta, i)di$ is the co-energy and has no physical significance. However, the torque is given by $\tau = \frac{\partial W_C}{\partial \theta}$. As seen in the figure, the magnetization curve is linear below the current i_{SAT}. Above this current the flux linkage begins to peak and *saturate*. Saturation is a condition that arises

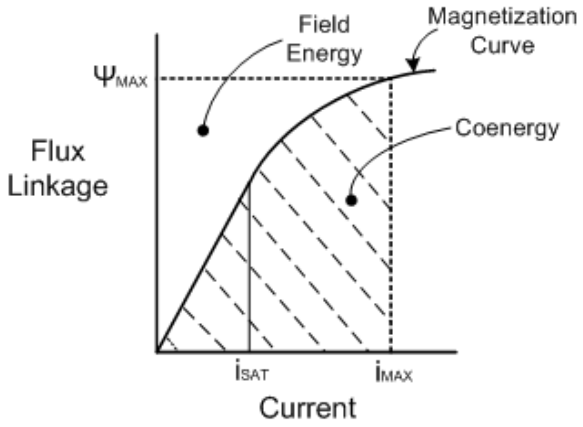

Figure 2.4: Flux Linkage vs Current

when the magnetic dipoles of the material have all aligned. When saturation occurs, the permeability of the material will begin to plateau at a minimum and approach the permeability of air.

The inductance of the motor may also be determined from the flux linkage, and is defined in Equation 2.3. The inductance, which is dependant upon geometry, pole number, windings and material properties through the flux linkage term, will ultimately determine the performance of the motor because inductance limits the controller's ability to govern the current and thus speed. A lower inductance translates to increased current control capability and vice versa. The inductance is given here as it is relates to SRM design and additional analysis presented in Chapter 4.

$$L(\theta, i) = \frac{\Psi(\theta, i)}{i} \tag{2.3}$$

As mentioned previously, the SRM is a doubly salient machine. In the traditional

SRM, inductance is primarily determined via self inductance as the rotor and stator poles do not overlap with other phases. Thus, there is not a flux linkage path, or it is at least negligible, between one phase and another. This lack of mutual inductance between phases results in a robust fault tolerant machine. This means that should a phase fail, the other phases are able to continue functioning with little effect to them. The motor's performance will suffer when a phase has failed, but the motor overall will not fail, and with sufficient phase count, the effect on performance may be acceptable as it will be able to "limp" along on the other phases. The motor is unaffected during a phase failure because the lack of mutual inductance between phases prevents back-emf from generating in the failed phase winding or controller causing additional damage to the failed winding or winding circuitry. The lack of mutual inductance also has drawbacks. As mentioned previously, the SRM has several issues concerning its wide spread usage, namely torque ripple and windage.

The torque produced by a machine may be computed by Equation 2.4 ,where θ is rotor position.

$$\tau(\theta, i) = \frac{\partial}{\partial \theta} \int_0^i \Psi(\theta, i) di \tag{2.4}$$

2.3 Conclusion

This chapter has described the basic theory and operation of the traditional SRM. Flux development and path through the SRM have been described as well as how

these produce useful torque. Throughout this chapter additional points necessary for understanding the new topology have been noted for clarity in the following chapters.

Chapter 3

JCRM Topology and Variations

The pursuant motor topology is referred to as the Johnson-Currie Reluctance Motor (JCRM) after the two developers, the author being one. This chapter details the physical layout and topology of the new motor. The layout given here was developed in parallel with the analysis of the motor given in Chapter 4. However, to understand the analysis given in the next chapter, the proposed motor configuration must first be understood.

As described in Chapter 2, the traditional SRM produces flux linkages in a plane or planes perpendicular to the axis of rotation, a radial gap topology. In this way, it can be said that the traditional SRM is essentially a two-dimensional machine. In fact, the SRM is typically analyzed as a 2D machine before multiplying by the depth to find the desired parameters. This geometric configuration for flux linkage is arguably the primary difference between the traditional SRM and the JCRM.

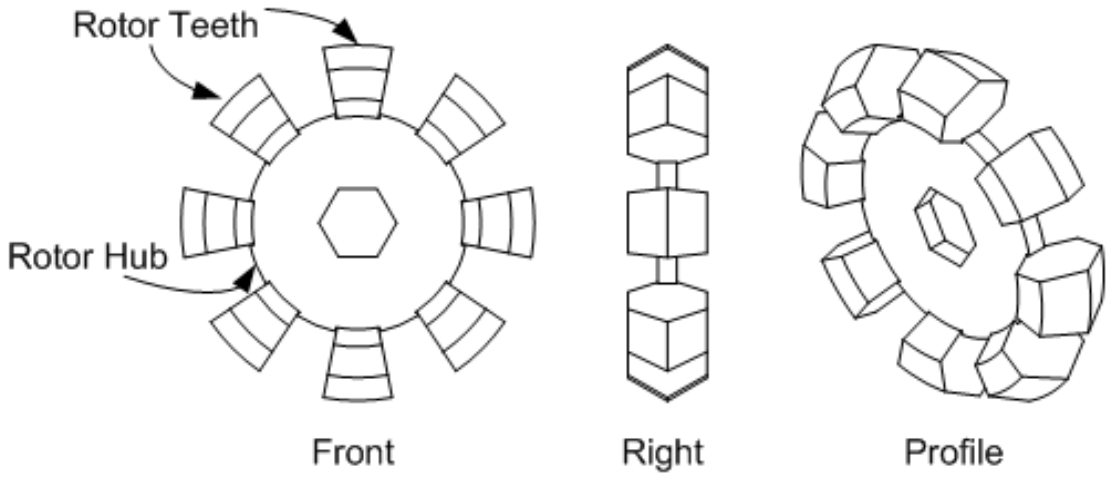

Figure 3.1: Rotor Body of the JCRM

To begin the description of the JCRM, Figure 3.1 shows the rotor *body* of the JCRM. The rotor body is not the traditional rotor yoke or rotor back iron as will be made apparent. While the rotor body is quite different from the traditional SRM rotor shown in Figure 2.2, its workings and purpose are similar.

The rotor body of the JCRM is composed of two sub-elements, the rotor hub and multiple rotor teeth. The purpose of the rotor hub is strictly mechanical integrity while the rotor teeth are composed of a magnetically permeable material. Unlike the traditional SRM, the rotor hub of the JCRM is not designed to be part of the primary flux path, instead, only the rotor teeth are intended to carry flux.

The rotor teeth, Figure 3.2, are held in place by rotor bands shown in Figure 3.3. The rotor hub, rotor teeth and rotor bands form the complete rotor assembly. The bands are internally tapered to hold the rotor teeth.

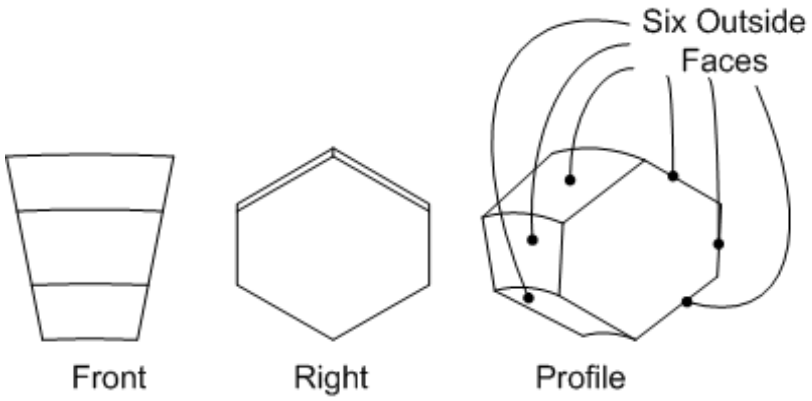

Figure 3.2: Rotor Tooth with Six Outside Faces - Toroid Segment

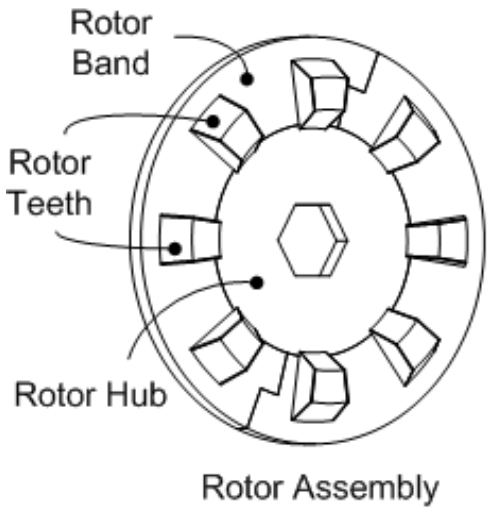

Figure 3.3: Rotor Assembly

Figure 3.2 shows a rotor tooth with six exterior faces. Note that these faces are of differing angular widths and lengths and thus all have differing surface areas. As flux will be passing through each face, it is important to have the area of each face equal or nearly equal. This equal area criterion will be detailed further in a later section as it is a crucial element of a successful design.

The rotor teeth are designed such that their spatial and angular offsets are symmetric and, as observed from Figures 3.2 and 3.1, can be loosely described as segments of a toroid. Flux paths, as in traditional SRMs, go between the stator and rotor teeth before traversing through the rotor and stator elements. However, in the JCRM topology, flux from the stator to the rotor is designed to primarily link the rotor teeth, not the rotor hub or rotor yoke as done in a standard SRM.

Surrounding the rotor teeth are stator *chucks*. Notice that the two chuck sets differ in Figure 3.4. The chuck set on the left has an enlarged and diminished chuck while the set on the right has mirrored chucks. These chuck sets are for the same motor but are utilized in different phases and/or arrangements. Arrangements of chuck sets are angularly and spatial offset from the rotor teeth and other stator chucks. The chucks shown in Figure 3.4 are for an overlapped design, thus the spacing between the chuck poles is equal to a chuck pole. Overlapped designs and spacing are described in further detail in Chapter 4.

The stator chucks are the primary flux conduit for the stator and are profiled such that their pole faces are made parallel to the rotor tooth face. Each chuck set, as

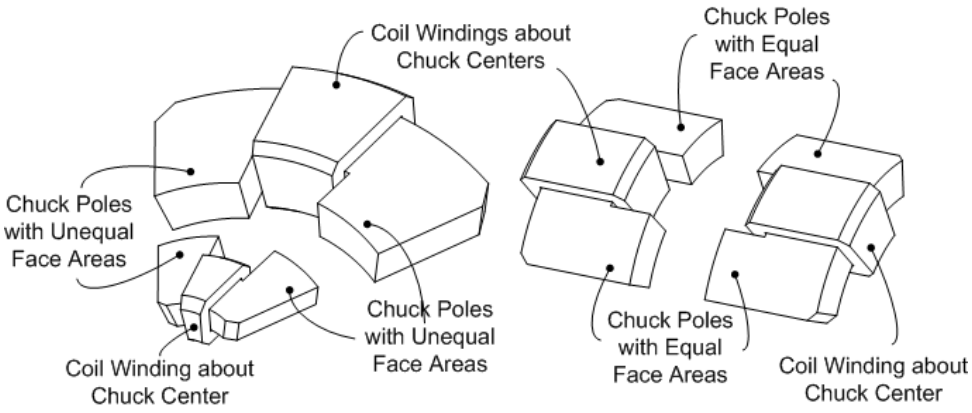

Figure 3.4: Two Different Complimentary Chuck Sets

shown in Figure 3.4, consists of two complementary chucks, each chuck having a pole pair.

An *arrangement* of stator chucks consists of one or more complementary chuck sets whose locations enclose and surround the rotor teeth. The term arrangement refers to the collection of chuck sets encompassing a particular angular and spatial offset. The right and profile views of three different arrangements are shown in Figure 3.5.

These arrangements when combined form a complete JCRM motor. Note the angular offset of the arrangements is done in such a manner that the arrangements enclose the rotor teeth. Also note that the first and third arrangements are physically identical although they are spatial and angularly offset differently. In fact, all arrangements are offset angularly and spatially to other arrangements. Just as standard phases are identified by their offset, i.e. Phases A, B and C all offset by 120° yet

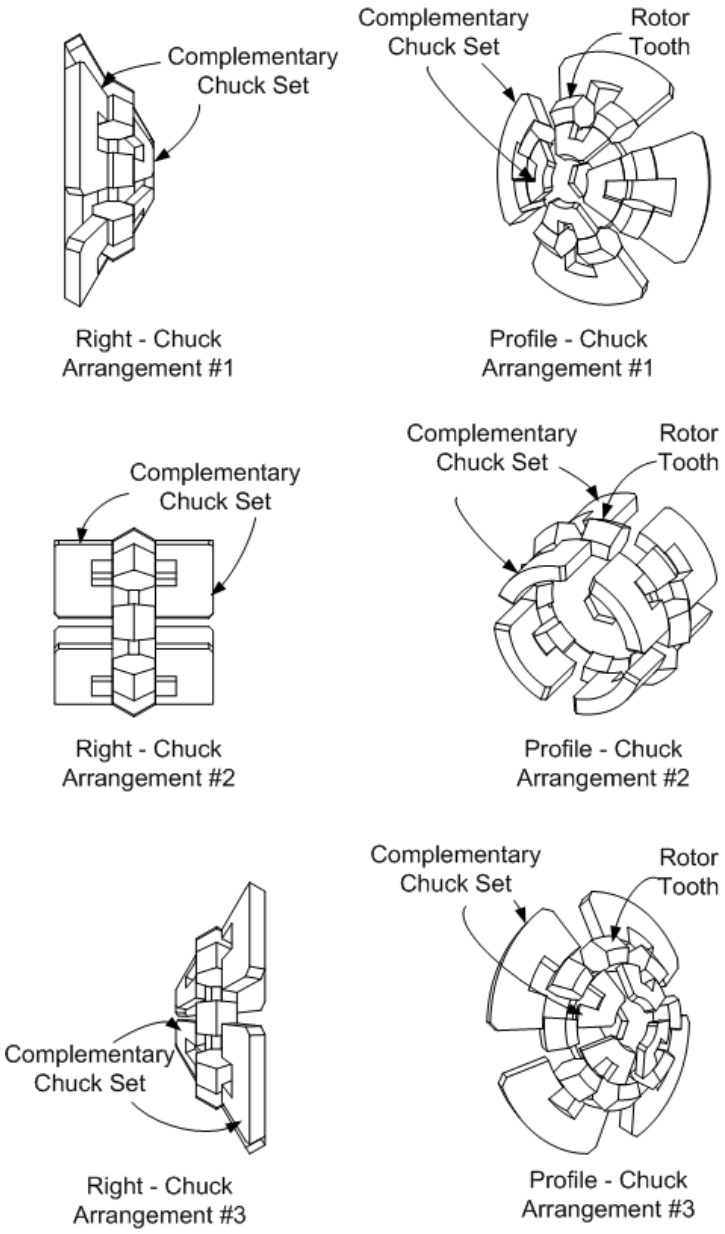

Figure 3.5: Various Chuck Arrangements

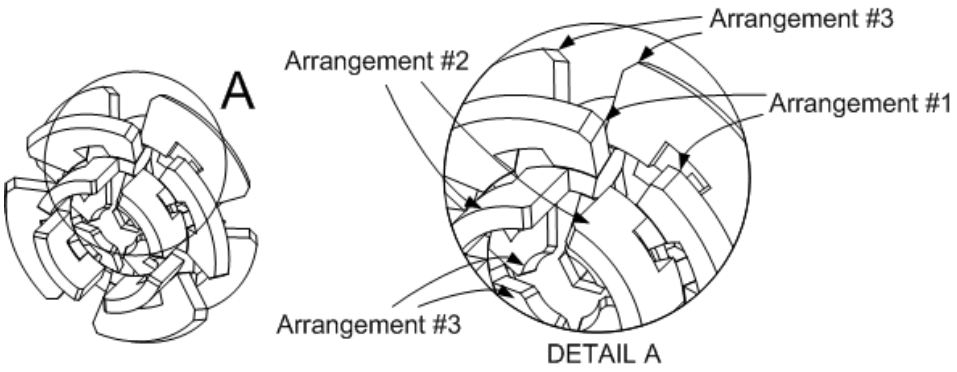

Figure 3.6: Three Different Chuck Arrangements Showing Angular and Spatial Offsets

are identical otherwise, arrangements are identified by their angular and spatial offsets. Figure 3.6 shows a completed JCRM motor (without windings) which includes three arrangements composed of four chuck sets each as shown individually in Figure 3.5.

As shown in Figure 3.6 the arrangements are located such that they partially overlap the rotor tooth with other arrangements simultaneously. Multiple schemes exist for overlap and will be addressed further in Chapter 4.

Figure 3.6 shows a complete JCRM without windings or housing. The figure shows three chuck arrangements and their angular and spatial offsets to stationary rotor teeth. Notice that the first arrangement is perfectly aligned with the rotor tooth in the figure while the second and third arrangements are only partially aligned with the tooth. By design, the arrangements overlap a portion of the rotor teeth, thus they overlap other arrangements. The stator chuck arrangements are held fixed by features that are integrated into a stator housing, shown in Figure 3.7.

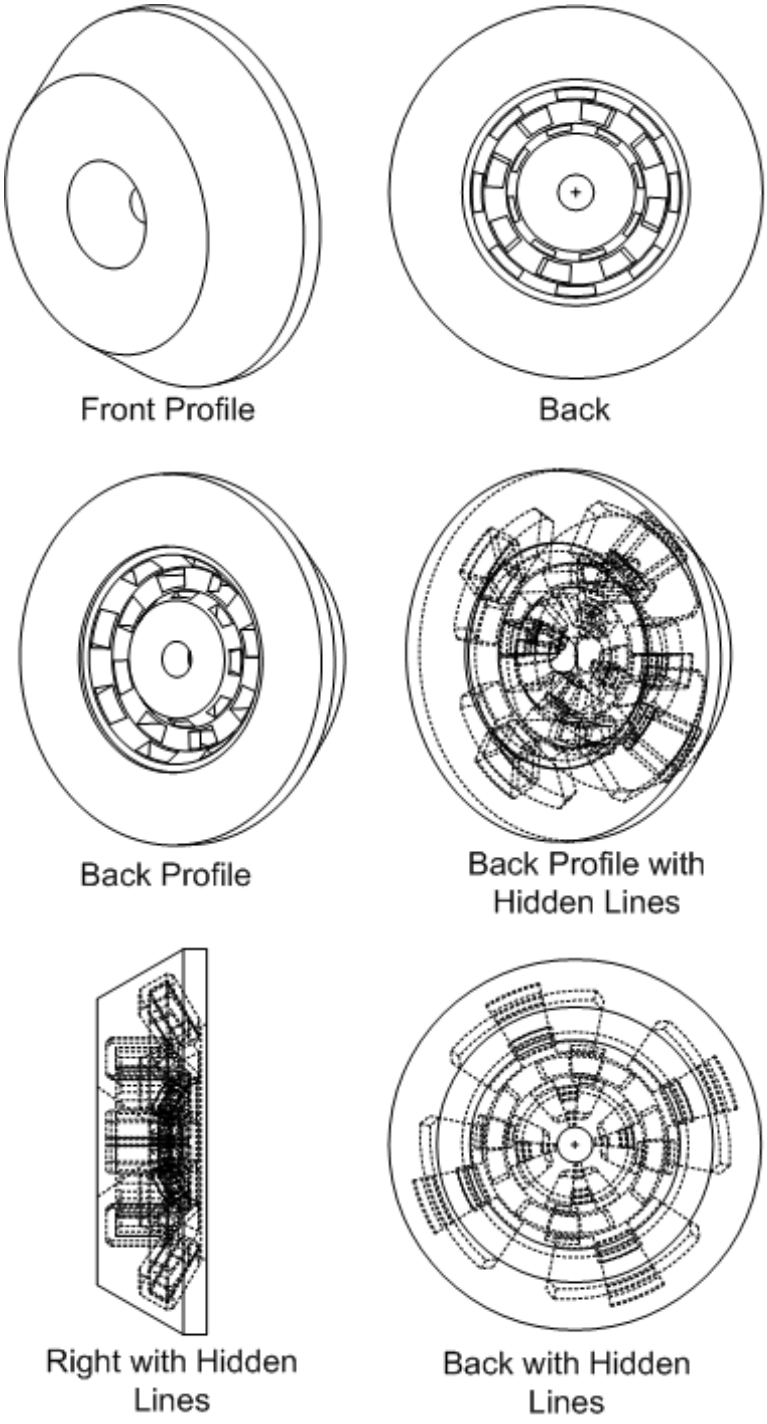

Figure 3.7: Stator Housing - Showing Half

Traditionally, the stator yoke acts as not only a flux conduit, but also as the housings for the motor giving it its mechanical integrity. As the flux path for the JCRM does not include the housing, it may be made of conceivably any material able to meet the application requirements, thus high grade plastics or even low grade aluminum are possible housing materials. In addition, because the windings are bound around the chucks which are discrete units, thus they are now able to be removed individually should a winding fail. This capability is unique to the JCRM and of great value to industry as this particular motor does not have to be removed from its location for repair.

3.1 JCRM Configurations

As flux linkage is established between one arrangement and the rotor teeth, the rotor teeth which are coupled to the rotor hub, will tend to align with the flux establishing arrangement. As the rotor revolves, the teeth begin to align with a new stator chuck arrangement as the new stator chuck arrangement is angularly and spatially offset from the initial arrangement, as shown in Figure 3.6. The new stator chuck arrangement then begins to establish new flux linkages as the torque peaks and begins to decay on the initial arrangement. This process of flux establishment, alignment of rotor teeth and chucks, flux decay and new flux establishment is repeated for continuous rotation and operation as the arrangements work cooperatively to successively initiate flux linkages from one stator chuck arrangement to another. As the stator chuck

arrangements are positioned angularly and spatially around the rotor teeth, flux linkage, and thus torque generation, is made along a three-dimensional path surrounding the rotor teeth, thus the torque is produced in a three-dimensional manner.

3.2 Loop Configuration

Thus far, the *loop* arrangement configuration has been shown in previous figures. This configuration would be ideal for applications with variable load because with sufficient control capability chuck sets, oppositely paired for symmetric torque production, could be disengaged. This would reduce the torque capability of the motor, but at the same time also reduce the power requirements and allow the remaining operational chuck sets to work in a more efficient, saturated, range of operation. In this configuration multiple flux paths exist within a chuck arrangement. The flux paths are localized about multiple, separate center points. Figure 3.8 shows four flux paths contained within the four chuck sets composing the arrangement. In Figures 3.8 and 3.9, the flux paths of a whole motor would involve two stator chucks per path, four flux paths per arrangement and one arrangement per phase for the particular motor detailed. As described previously, Figure 3.9 shows that the top layer chucks have complementary chucks to the opposite side bottom layer, showing angular variation, and each chuck set is spatially offset from the other sets, showing the spatial variation.

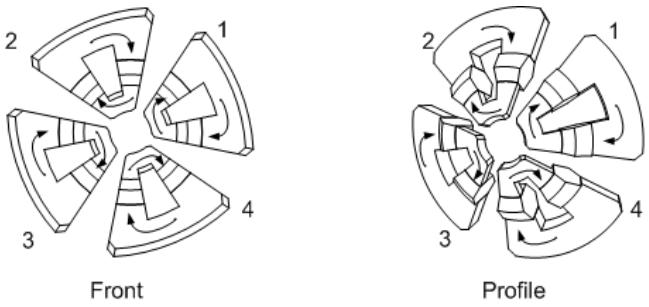

Figure 3.8: A Single Chuck Arrangement in "Loop" Configuration

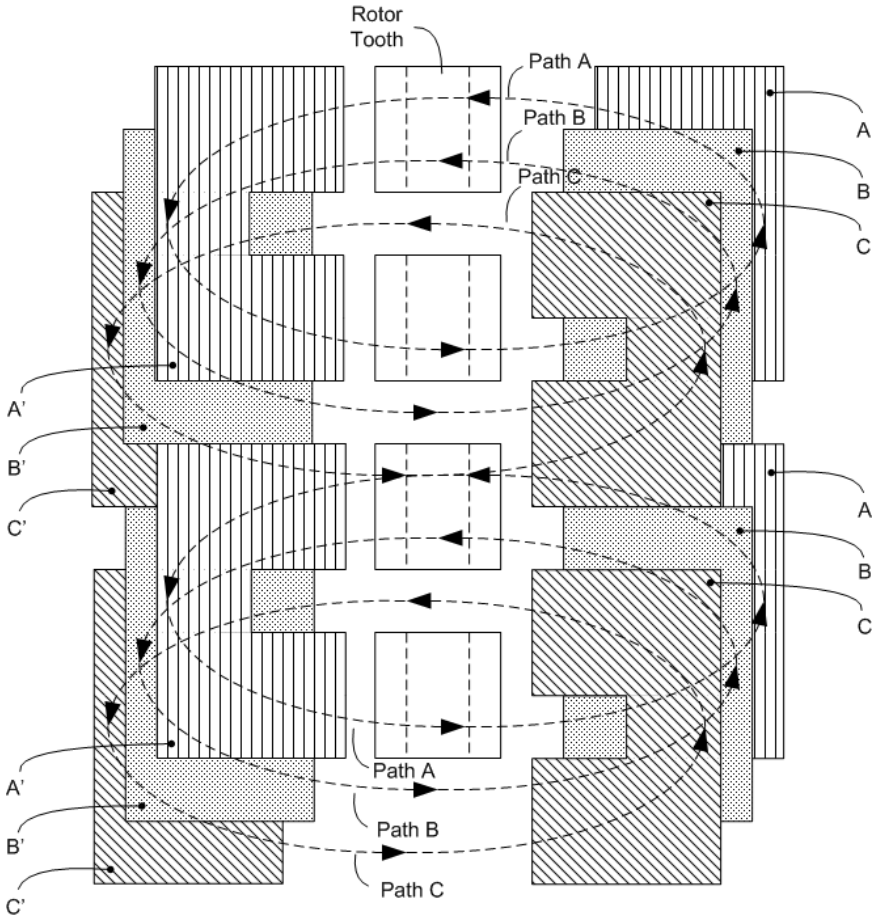

Figure 3.9: Layout Diagram of Loop Configuration

3.3 Coupled Configuration

Figure 3.10 shows the *coupled* configuration in which a single primary flux path between all chucks in an arrangement exists, while Figure 3.11 shows the layout when three stator chuck arrangements are combined. The coupled configuration would be ideal for applications with roughly constant loads as flux linkage is maximized due to the series nature of the chucks. In addition, with sufficient controls, a failed winding on a chuck could be disengaged, yet as the chuck still lies in the flux path the remaining phase windings of the arrangement continue to operate and allow the arrangement as a whole to continue operating. This particular configuration has not been analyzed further and is presented here simply to show that other possibilities exist for future work.

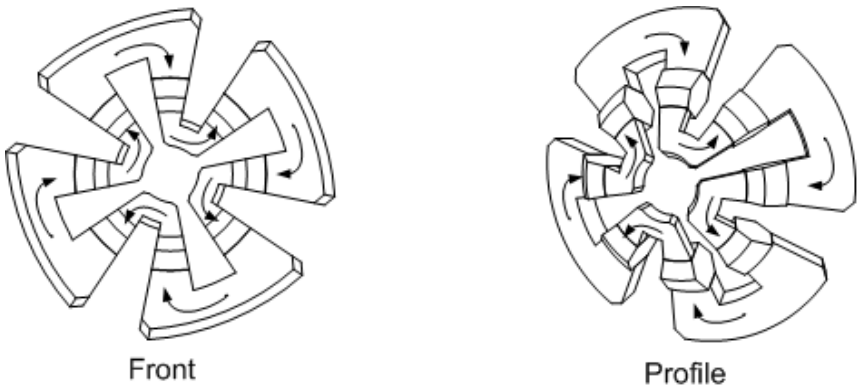

Figure 3.10: A Single Chuck Arrangement in "Coupled" Configuration

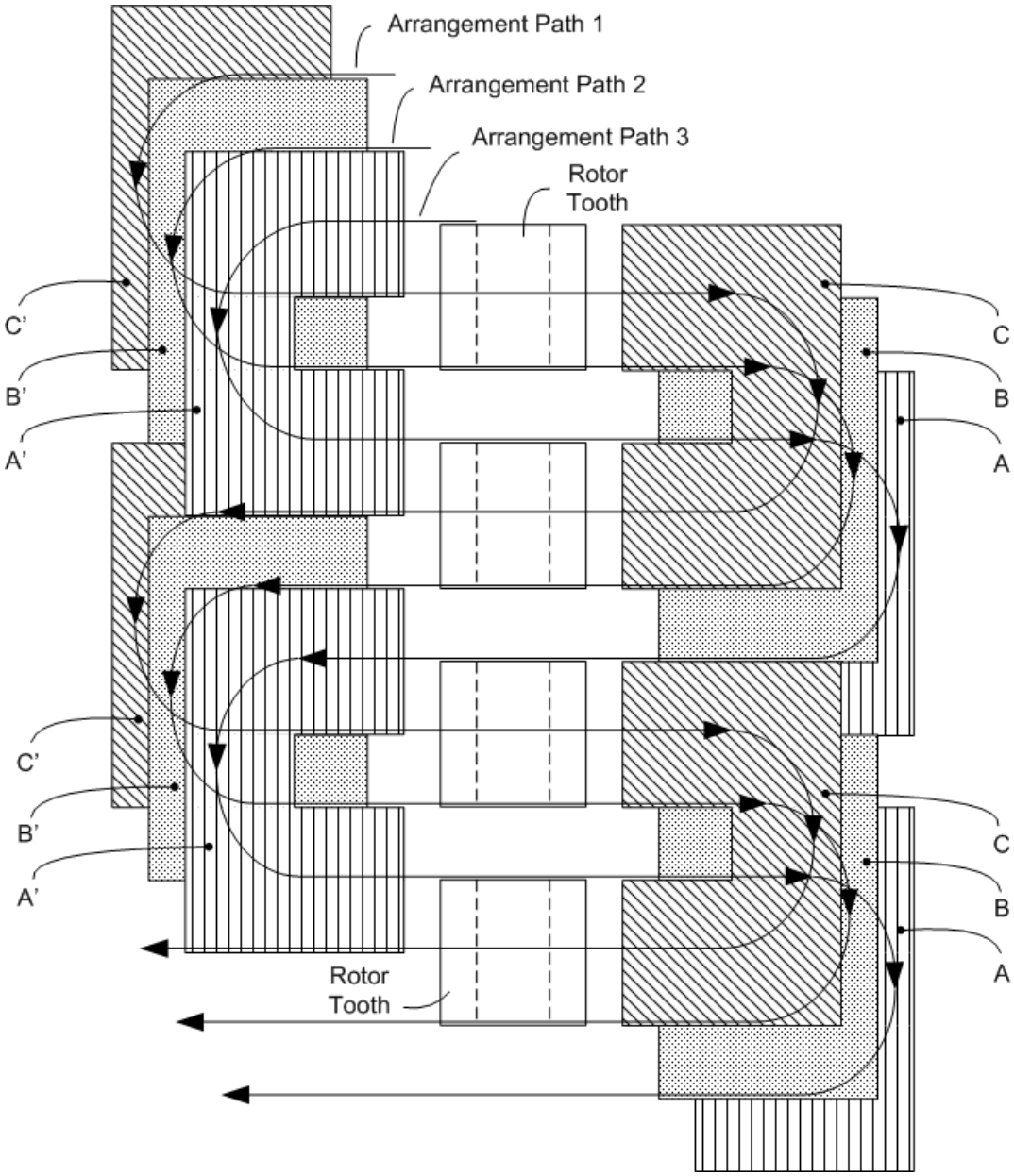

Figure 3.11: Layout Diagram of Coupled Configuration

3.4 Flux Linkage Transitions

Independent of the configuration, transitioning of flux linkage from one stator arrangement to another, occurs in a rotating manner within the rotor tooth. The transitioning from one stator arrangement to the next is shown in Figure 3.12. The arrows indicate the primary direction of the flux path within a stator tooth. If there is little to no overlap, the previous primary arrangement may have little effect upon the developing linkages.

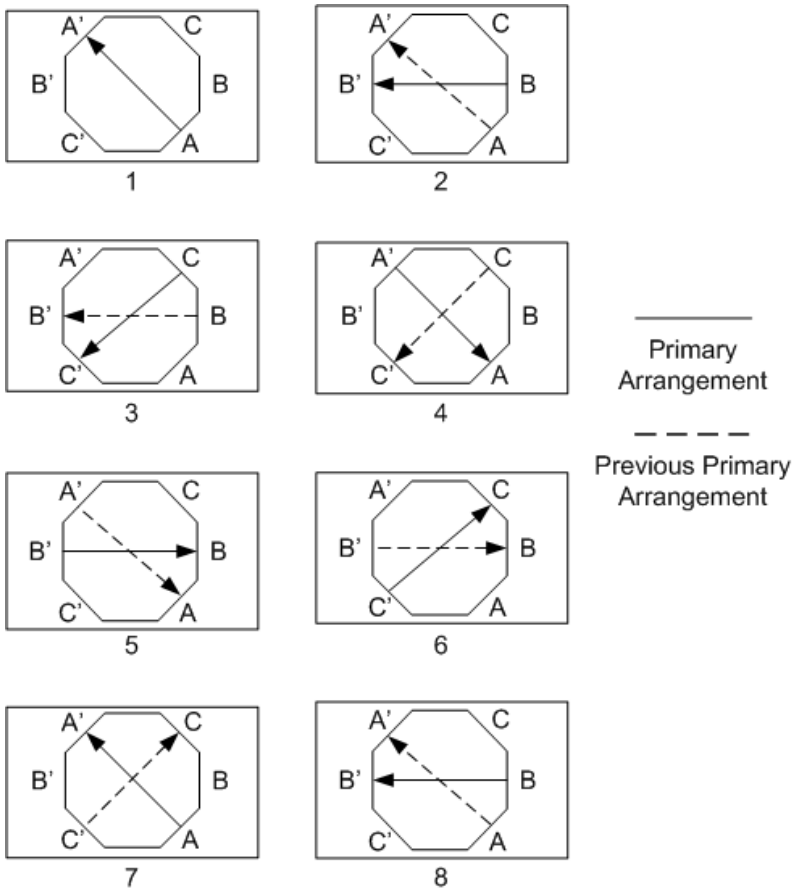

Figure 3.12: Flux Linkage Transition with Three Stator Arrangements

3.5 Overlap and Sizing

With the utilization of three-dimensions for torque production, each rotor tooth is now accessible for utilization during each commutation step thus increasing the utilization of the available material. However, a three-dimensional profile implies that a single phase machine is unlikely because a flux gradient, necessary for torque production, within the single phase would be difficult to construct. Although, it may be possible to combine the JCRM and a PMM to produce a single phase machine of this topology.

The number of rotor teeth is defined by the number of chucks ($N_{Teeth} = 2 * N_{Chuck}$). While the number of teeth is quickly defined, the angular positioning of the chuck arrangements requires greater attention. Figure 3.13 shows three different scenarios for rotor and stator spacing. This figure is intended to highlight the various possibilities and resulting rotor tooth spacing. For the top example with 0% overlap, notice that the rotor teeth must be spaced at twice their width. This would result in a rotor tooth to spacing ratio of 1:2 or 0.5. For the 25% overlap example, the ratio increases to 1:1.25 or 0.8. In the final example with 30% overlap the ratio peaks at 1:1.

Figure 3.14 gives the resulting spacing ratios for the non-overlap (0%) scenarios. Notice that as the phase count increases the spacing of the rotor teeth becomes extreme and unfeasible. Thus, high phase count non-overlap scenarios are impractical with the JCRM topology.

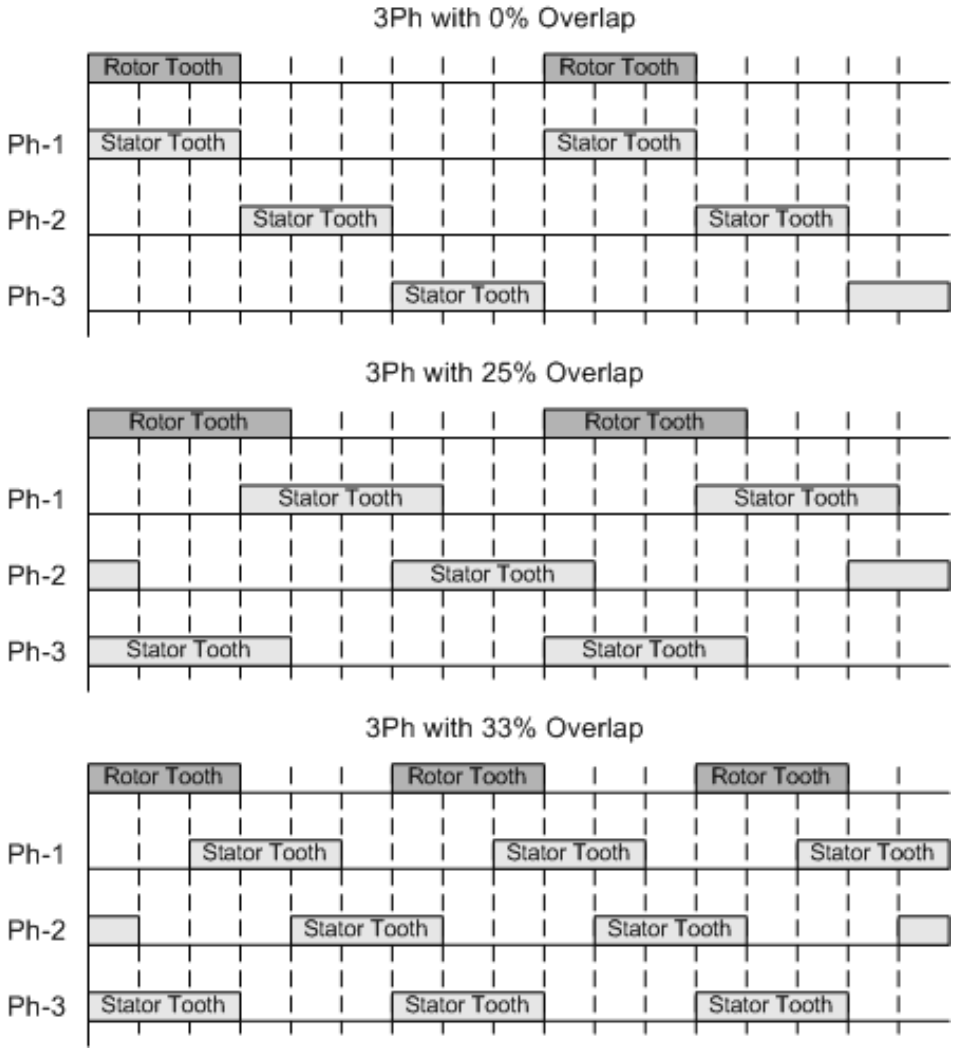

Figure 3.13: Overlap Possibilities of a 3Ph Motor

Phase	Spacing Ratio	Spacing Fraction	Overlap Pattern
2	1:1	1	1:1:1:1
3	1:2	0.5	1:1:1:1
4	1:3	0.3	1:1:1:1
5	1:4	0.25	1:1:1:1
6	1:5	0.2	1:1:1:1
7	1:6	0.166	1:1:1:1

Figure 3.14: Non-overlap Relations

For scenarios that allow overlap refer to Figure 3.15. For overlap scenarios the ideal spacing ratio is exactly 1:1. Ratios less than this, as in the 25% overlap case, are an inefficient usage of space and material. For overlap scenarios it is also interesting to note the overlap pattern and %-overlap of the rotor by the stator teeth. (The overlap pattern is the number of phases that could act upon the rotor tooth at any given time.) Notice that the odd phases have an overlap pattern that is discontinuous, varying in the number of overlapped arrangements, while even numbered phases have a uniform overlap pattern. Notice also that as the phase number increases the %-overlap approaches one and is directly tied to the phase count. Finally, notice that the two phase overlap scenario does not exist meaning that its spacing is already maximized at the non-overlap condition.

Phase	Spacing Ratio	Overlap Pattern	% Overlap of Rotor
2	1:1	1:1:1:1	0/2
3	1:1	2:1:2:1	1/3
4	1:1	2:2:2:2	2/4
5	1:1	2:3:2:3	3/5
6	1:1	3:3:3:3	4/6
7	1:1	3:4:3:4	5/7
8	1:1	4:4:4:4	6/8

Figure 3.15: Overlap Relations

3.6 SRM and JCRM Topological Differences

The traditional SRM flux path is through a salient stator tooth, then a salient rotor tooth, then a rotor yoke, then an additional salient rotor tooth, then an additional salient stator tooth, then a stator yoke before returning back to the originating stator tooth. This flux path lies within a plane (commonly modeled via a two-dimensional layout) perpendicular to the axis of shaft rotation. The new topology expands the realm of reluctance motor design. The new motor topology has a flux path that traverses a stator chuck's center, then through the stator chuck's pole, the rotor tooth, the complementary stator chuck, then through another rotor tooth, then either the originating chuck pole or a different chuck pole, depending upon the configuration, loop or coupled.

The JCRM topology creates a flux path that is in a plane transverse (other than) to the rotation plane.

3.7 Primary Differences between the Traditional SRM and JCRM

The differences between the JCRM and the standard SRM include:

1. Flux path is through the respective rotor teeth and stator chucks, not through the rotor and stator yokes. Thus, non-magnetic materials may be utilized in the construction of the motor housing and encasement.

2. Each rotor tooth is utilized in every phase engagement thus there is a higher utilization of available rotor material than with the traditional SRM design. This may help reduce the volume of the motor and material costs.

3. In transferring the torque production and flux path to a plane transverse from the axis of rotation, the windings are accessible for easy removal and replacement, an ideal maintenance feature as the motor does not have to be removed for repair or rebuild.

4. In transferring the torque production and flux path to a plane transverse from the axis of rotation, axial vibrations may now arise and present significant performance issue. Evidence to this effect is presented in Chapter 5 although further analysis is required.

5. Overlapped and non-overlapped configurations are possible with the JCRM topology.

6. Multiple chuck configurations (looped and coupled) exist for the JCRM allowing for possible tailoring of the motor to an application.

7. Increased geometric complexity of the JCRM and thus it has increased analytical complexity.

8. As the flux paths are not shared, the JCRM may weigh more than a traditional SRM as additional back iron is required.

3.8 Conclusion

This chapter has described the topology of the new reluctance motor, the Johnson-Currie Reluctance Motor. This topology has been shown to have diversity in its construction (loop and coupled, overlapped and non-overlapped) to meet numerous applications. A simple comparison has also been made to highlight the major differences between the traditional SRM and the JCRM.

Chapter 4

Design and Analysis

As stated at the beginning of the last chapter, an understanding of how the JCRM motor is constructed must preced the analysis and design of the motor. The analysis will then dictate the specifics of the motor. For this prototype motor, the overall governing design parameters will have several practical limits. It is desired to build a small prototype motor for lab testing and to function as proof of concept. It is desired that the prototype motor have three-phases (three stator chuck arrangements) and a maximum current of 3.5A.

4.1 Mechanical Design

Several additional design constraints must be defined prior to beginning the analysis. These design constraints are the number of chuck sets in an arrangement N_{Chuck_Sets}, the number of phases N_{Ph}, the diameter of the rotor (defined as the center of a rotor

tooth to an opposite rotor tooth center) R_{Dia}, and the effective rotor tooth height T_{eh} defined as the distance between two oppositely paired faces within a rotor tooth.

4.1.1 Rotor Tooth Design

The number of rotor teeth is given in Equation 4.1.

$$N_{Th} = 2 * N_{Chuck\_Sets} \tag{4.1}$$

With this, the angular spacing of the rotor teeth for a non-overlapping arrangement (switched reluctance) design is able to be determined and is given in Equation 4.2.

$$A_{Tooth} = \frac{2\pi}{N_{Th} * N_{Ph}} \tag{4.2}$$

The angular spacing between each tooth for a non-overlapping arrangement design is given in Equation 4.3.

$$A_{Space} = (N_{Ph} - 1)\, A_{Tooth} \tag{4.3}$$

For the overlapping condition (variable reluctance), the tooth and space angles are defined.

$$A_{Tooth} = \frac{\pi}{N_{Th}} \tag{4.4}$$

$$A_{Space} = A_{Tooth} \tag{4.5}$$

4.1.2 Flux Paths

Knowing the basic structure of the motor now allows for the operating parameters of the motor to be determined. In a manner similar to finite element analysis (FEA), typical paths for flux linkage are modeled and then iteratively solved for equivalence with known current and turns of the phase coils. This analysis begins with an understanding of the chuck set's magnetic path. In all, five flux paths have been described in an attempt to represent the major linkage paths for fringing and torque development.

The flux paths are described using the basic geometry of the motor and the assumptions that flux enters and exits an element normally, the rotor hub and rotor band are purely non-magnetic, and that flux lines within an element are parallel. As these electrical circuits model a magnetic circuit, the resistances represent reluctances of the material and the voltage sources represent magnetization force (H). These electrical circuits, given in the next section, represent the physical path for flux, from its generation in the windings ($\Sigma(H\ell) = NI$) which surround the chuck center, then through the chuck tooth, then rotor tooth, then complementary chuck, then another rotor tooth, then finally completing the circuit back at the initiating chuck and winding. Between the stator and rotor teeth is a physical gap. The gap insures the rotor is able to move freely and will not contact the stator. Ideally, this gap is as small as possible but due to variations in construction, the gap for this motor has been set at 0.4mm.

4.1.3 Algorithm Design

With an assumed rotor diameter, phase number and current limit, the remainder of the motor, geometry and operating characteristics may be determined explicitly. This algorithum has assumed that the flux traverses five primary paths.

Path 1

This path is located in the chuck inside corners and is strictly leakage flux, thus it does not contribute to useful torque production and is considered a loss yet will add to the inductance calculation. This path is due to the high saturation that occurs on the inside corners of the chucks. This path is marginally related to rotor position. For one chuck set, there are four inside chuck corners, this path is located in each of these corners and is shown represented in Figure 4.1 and by the electrical diagram in Figure 4.2. There will be two of these flux paths per chuck, only one is shown.

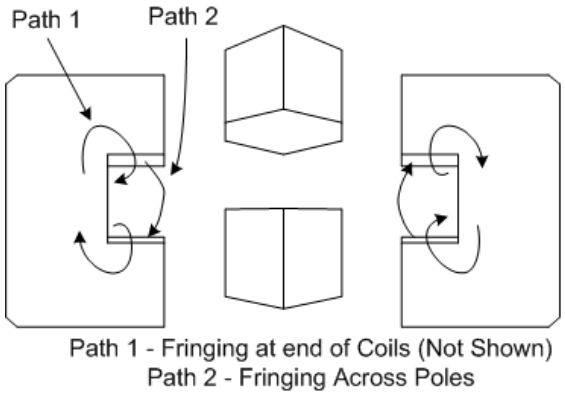

Figure 4.1: Flux Paths 1 and 2 in Chucks

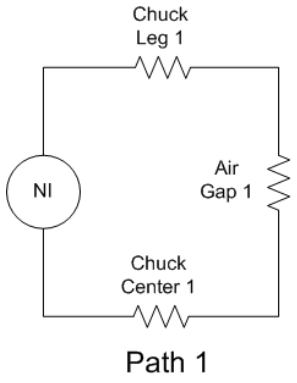

Figure 4.2: Flux Path 1 Electrical Diagram

Path 2

Flux path 2 is also a leakage flux path and is shown in Figure 4.1. Path 2 will have marginal dependance upon position yet in an inverse proportion. This is because the reluctance of this fringing path will actually increase as alignment occurs when compared to the primary flux paths described in the next section.

Path 2 traverses through a chuck center and partially up a chuck leg, then through the air gap between the two legs of the chuck. Flux will not normally cross this large air gap, however, the field around the winding provides a marginal bridge between the two legs, obviously increasing in strength as current through the winding increases. As with Path 1, the height of this flux path, up the chuck leg, is marginally dependant upon rotor position. Saturation of the chuck will have will direct effect upon this path as the air gap is between the chucks is relatively large. The electrical schematic for this path is shown in Figure 4.3.

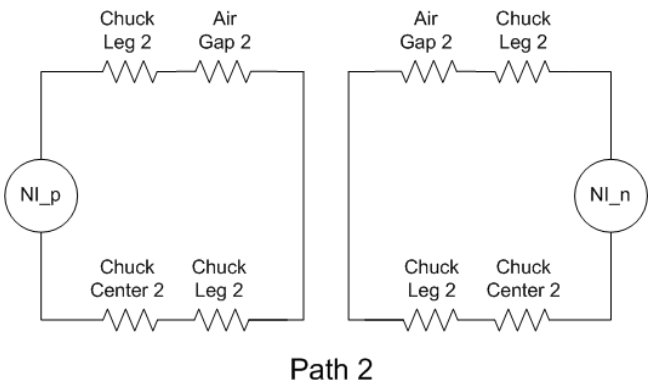

Figure 4.3: Flux Path 2 Electrical Schematic

Path 3

Flux path 3 is the primary flux path and thus the primary torque producing path. This path goes thorough all elements and is centered in each element through the overlapping areas. This path is highly dependent upon rotor position and current as expected.

Path 3 traverses the stator tooth/rotor tooth air gap through a 2D plane, going from the chuck leg face directly to the rotor tooth face. Because of this direction path from one face to the next it is thus the primary flux path. The path length will vary with the rotor toth position as it has been assumed that the path will moves to maintain average position in the center of each of the overlapping faces. This condition occurs regularly with traditional 2D motor designs and thus believed to be a good assumption here as well. The physical representation is shown in Figure 4.4 and the electrical schematic for this path is shown in Figure 4.5.

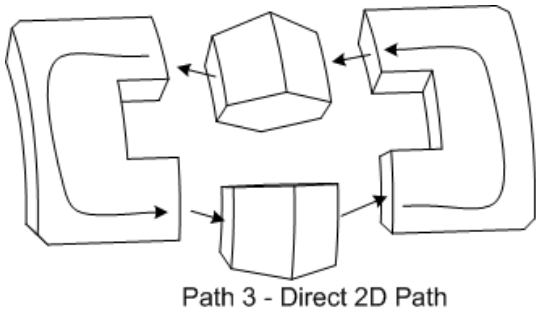

Figure 4.4: Chuck Path 3

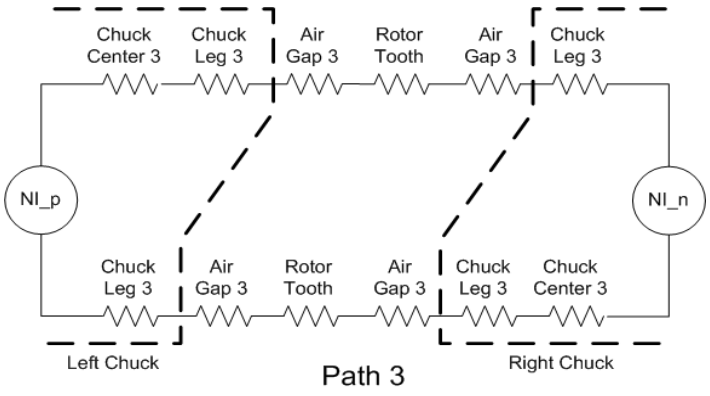

Figure 4.5: Flux Path 3 Electrical Schematic

Path 4

Flux path 4 represents flux that does not enter or exit the stator chuck directly from the front of the chuck tooth face. Instead, the flux of this path enters and exits from the sides of the tooth. The flux path is dependant upon rotor position, being largest during unalignment and disolving to a marginal value during alignment as the primary flux will be through the tooth face during alignment. This path is shown in Figure 4.6 and is represented by the electrical schematic shown in Figure 4.7.

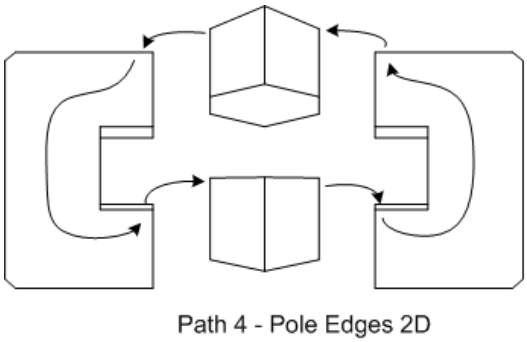

Figure 4.6: Chuck Path 4

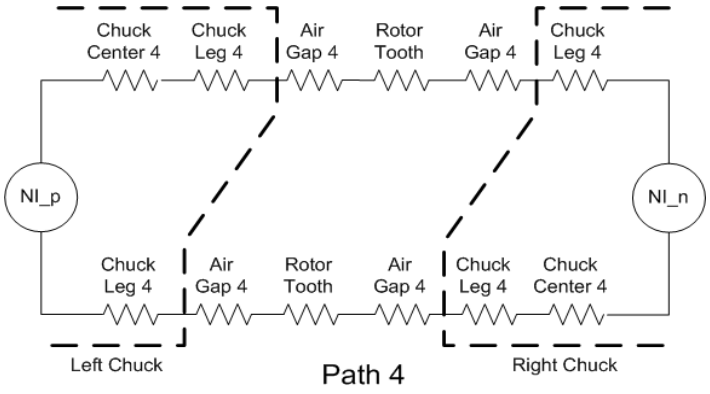

Figure 4.7: Flux Path 4 Electrical Schematic

Path 5

Flux path 5 is the only true 3D path. This path passes through the chuck, exiting the chuck tooth face but then moves to a face other than the face for the engaged phase, taken by Path 3. This path is symmetic as is splits and traverses to both the rotor tooth face above the one taken in Path 3 and the face below. Is is assumed that the flux enters and exits the faces normal to each face. This path is shown in Figure 4.8 and is represented by the schematic shown in Figure 4.9.

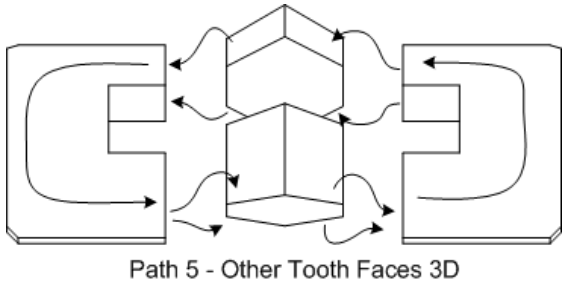

Figure 4.8: Chuck Path 5

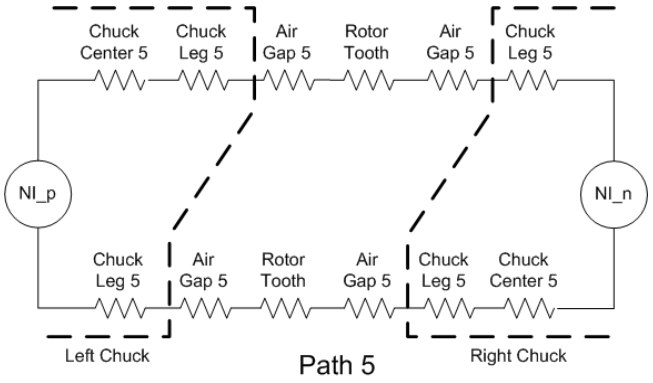

Figure 4.9: Flux Path 5 Electrical Schematic

Now with these constraints defined, the input parameters by which the motor may be analyzed are complete. However, these constrains will need to be adjusted as additional information, namely that of FEA, becomes available to insure accurate modeling of the motor and its flux paths.

The algorithm starts initially by computing the geometry for the motor based upon user input, rotor diameter, rotor tooth size, number of chucks, etc. The algorithm then makes an assumption for the B field in the chuck center of a phase. The motor characteristics are solved by the following algorithm shown in Figure 4.10.

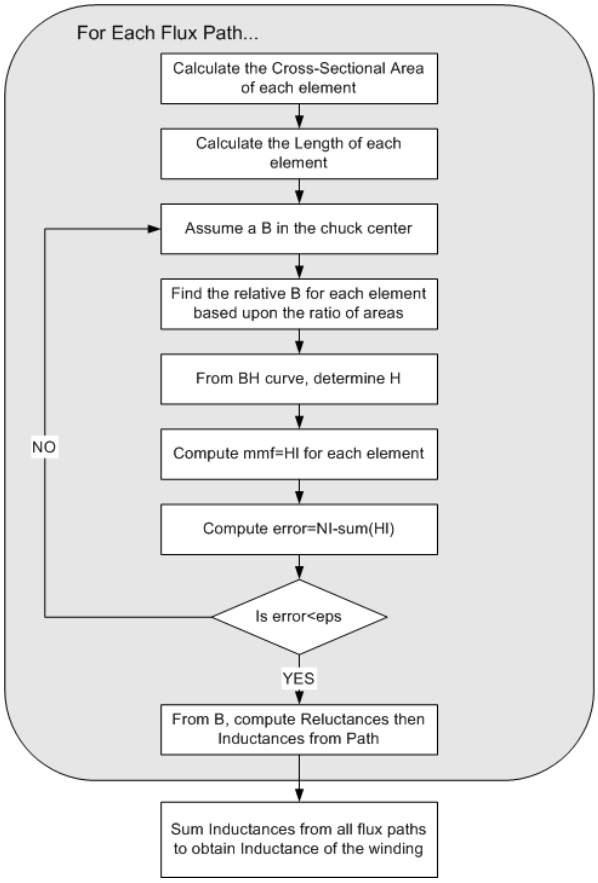

Figure 4.10: Flux Path Algorithm for Computing Motor Characteristics

Using a ratio of the cross-sectional areas for each element as shown in Equation 4.6, the B field through each path may be found.

$$B_k = B_{chuck\_center}\frac{A_{chuck\_center}}{A_k} \tag{4.6}$$

Once the B field is computed, the field intensity, H, is found from the material's B-H curve for each element. The mmf of the path is then computed and compared to the input as shown in Equation 4.7.

$$NI = \sum_{k=1}^{\#elements} H_k \ell_k \tag{4.7}$$

If the right side equals the left in Equation 4.7 then the assumed B field is correct. If the two do not equal, then the assumed B field is incremented slightly. This process is continued for each path and for each phase until all the B and H fields are known. Once known, the reluctance for each element is computed from which the inductance and flux linkages can be determined using Equations 4.8, 4.9 and 4.10.

$$\Re = \frac{H\ell}{BA} \tag{4.8}$$

$$L = \frac{N^2}{\Re} \tag{4.9}$$

$$\Psi = Li \tag{4.10}$$

4.2 Conclusion

This chapter has described the methodology undertaken by which the JCRM has been designed and analyzed. The method of analysis, defining flux paths and their movement based upon rotor tooth positioning, has been described along with the algorithm for computing the motor's performance characteristics.

The following chapter describes the results of the simulation using the described algorithm and FEA comparison.

Chapter 5

Results of Simulation and FEA Comparison

A MATLAB program was constructed to analyze the JCRM topology through various parameter changes. During the development of the program it was the intent to keep the program generic, allowing for any phase number, rotor diameter, chuck number, rotor tooth size or ranges thereof could be entered as parameters for the program to compute.

Based upon geometry, a number of relations can be determined to help improve the design. Figure 5.1 shows how a variation of rotor diameter modifies the rotor tooth area ratio ($\frac{smallest\_area}{largest\_area}$) with larger ratios being ideal. This relation is important as it is clearly shown that smaller rotor teeth and larger diameters are preferred.

Additionally, it is also important to gauge the effects of the effective tooth height

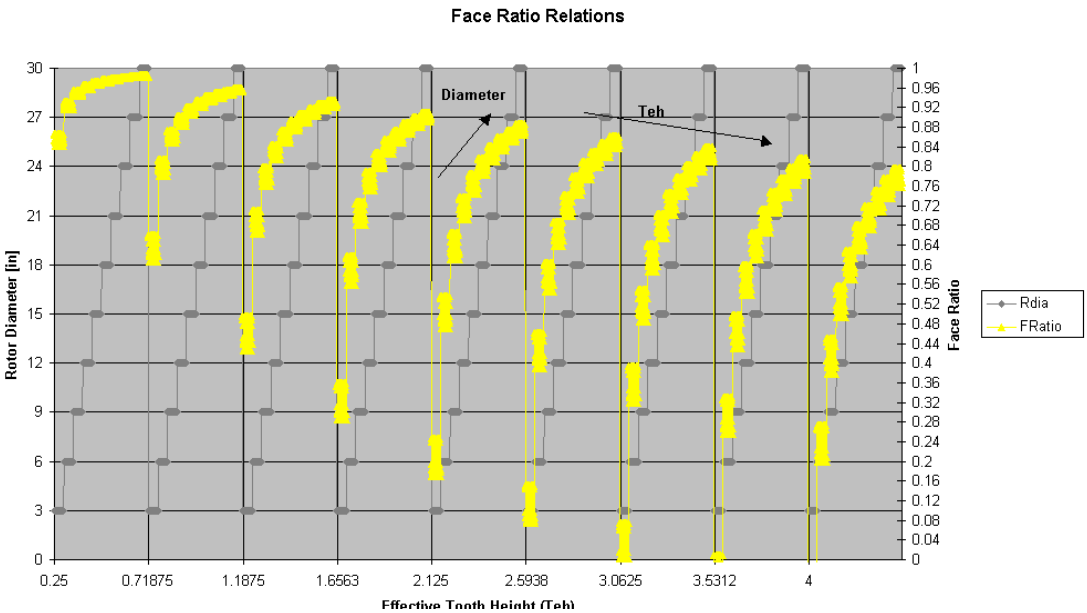

Figure 5.1: Relations of the Face Ratio

upon the overall motor volume. Figure 5.2 gives these relationships. Figure 5.2 must be used in conjunction with Figure 5.3 which together show that large diameter motors with low chuck counts result in large volumetric motors. The volume grows quickly as the relation of the tooth width to height, computed earlier, must be maintained.

A final relation that is able to be extracted from the geometric relations and helpful in the design is to understand the winding count relations. Figure 5.4 shows how the number of turns of 16AWG grows (meaning the area between chuck poles) as the rotor diameter grows. Notice again, that as the chuck number increases the winding count decreases. It would be impractical to construct a motor with such high turns count as the inductance and thus back-emf would be severe, however, the relationship between the turns, diameter and chuck count is understood.

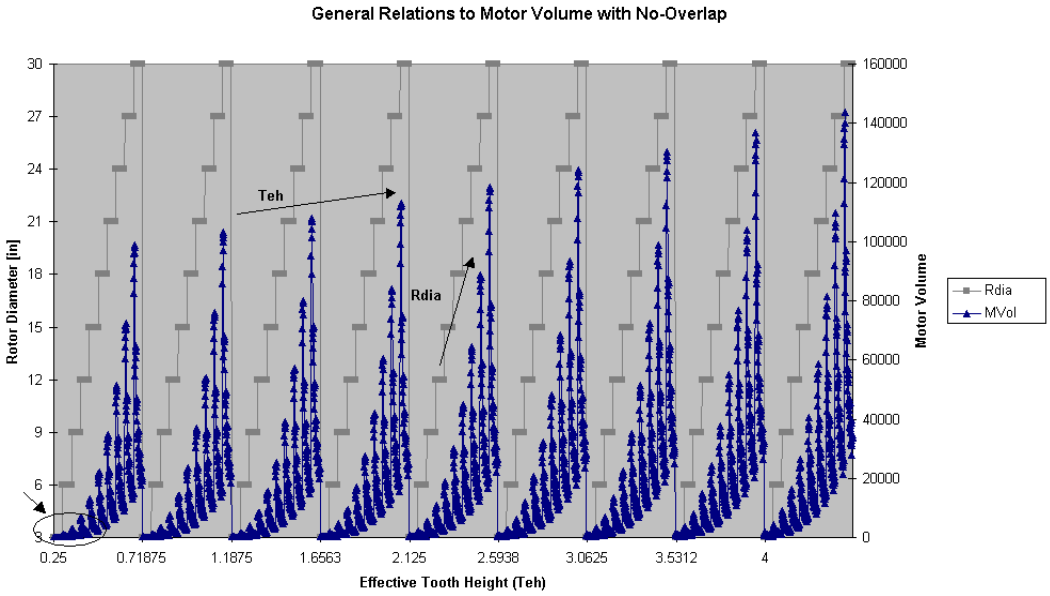

Figure 5.2: General Volume Relations

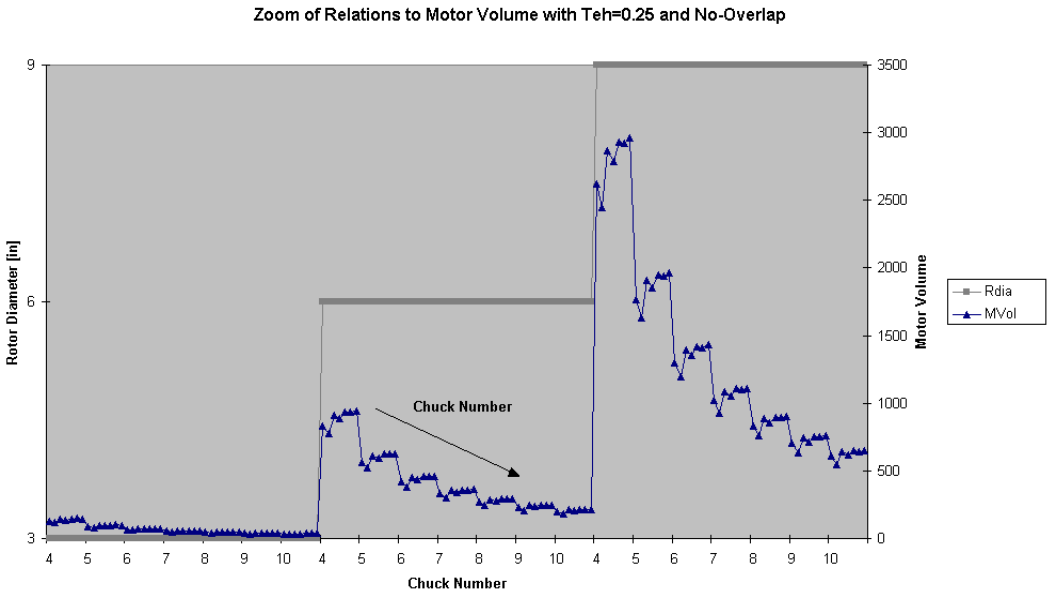

Figure 5.3: Zoom of Volume Relation

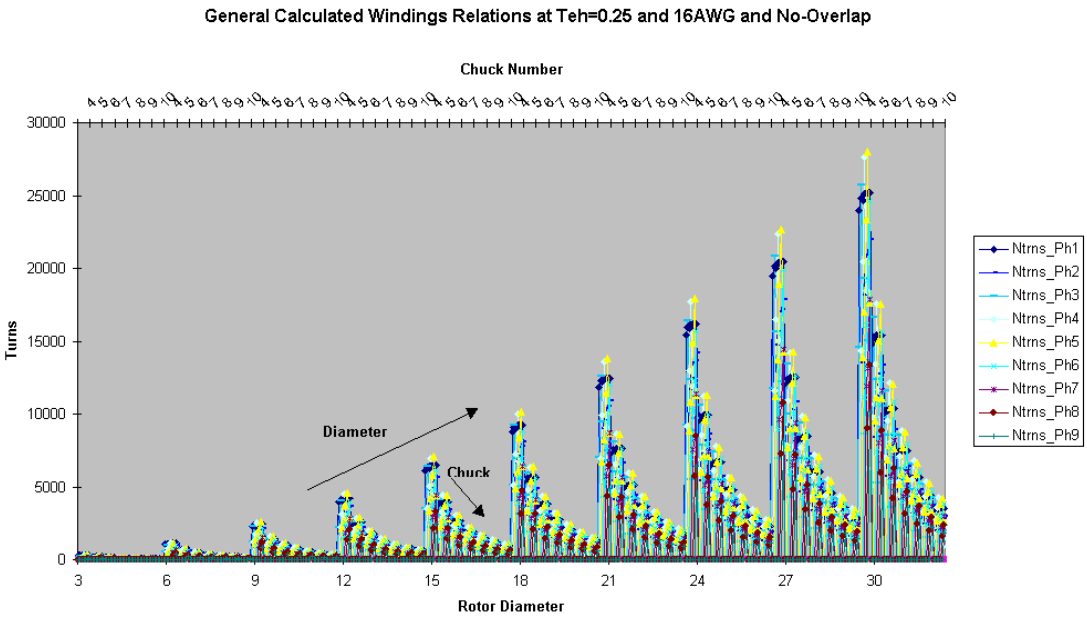

Figure 5.4: Winding Relations

From Figures 5.1 and 5.2, general design relations can be established. Ideally, the JCRM would have a small tooth height, large diameter and high chuck count. In doing so, the motor should result in a high face ratio, low volume motor. However, as with all engineering problems, these must all be balanced against design and construction complexity and motor performance parameters to reach a premium design. As this is a prototype motor intended for future construction with additional refinement, a three inch diameter, three phase motor, four chuck with no-overlap has been chosed for analysis so that the performance characteristics can be gauged upon experience and available SRMs for comparison and baseline testing.

Figure 5.5 shows the resulting flux linkage plots from a non-overlapping design

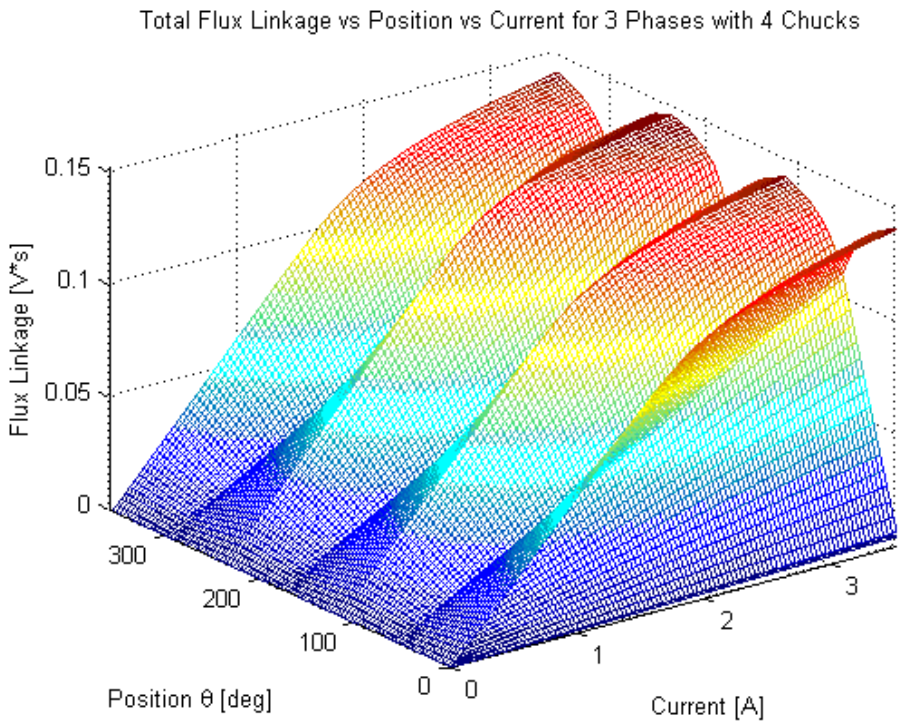

Figure 5.5: Flux Linkage for 3-Phases at 3.5A with 4 Chucks and Non-Overlapped

incorporating three phases, four chucks, with a three inch diameter and a maximum current of 3.5A. From the figure, notice that the effects of saturation are shown for currents above 2A roughly, as the flux linkage slope decreases.

From this plot it is worth noting that the curves are not perfectly symmetric, as seen by the higher and lower peaks, thus, it is truly necessary to analyze all three phases. The phase plots are not identical as the flux paths are not identical in length nor are they necessarily identical in cross section. As mentioned in Chapter 3, the rotor tooth has different faces for each phase. If the face ratio is not close to unity, then the flux path is likely to saturate earlier in an electrical rotation than another

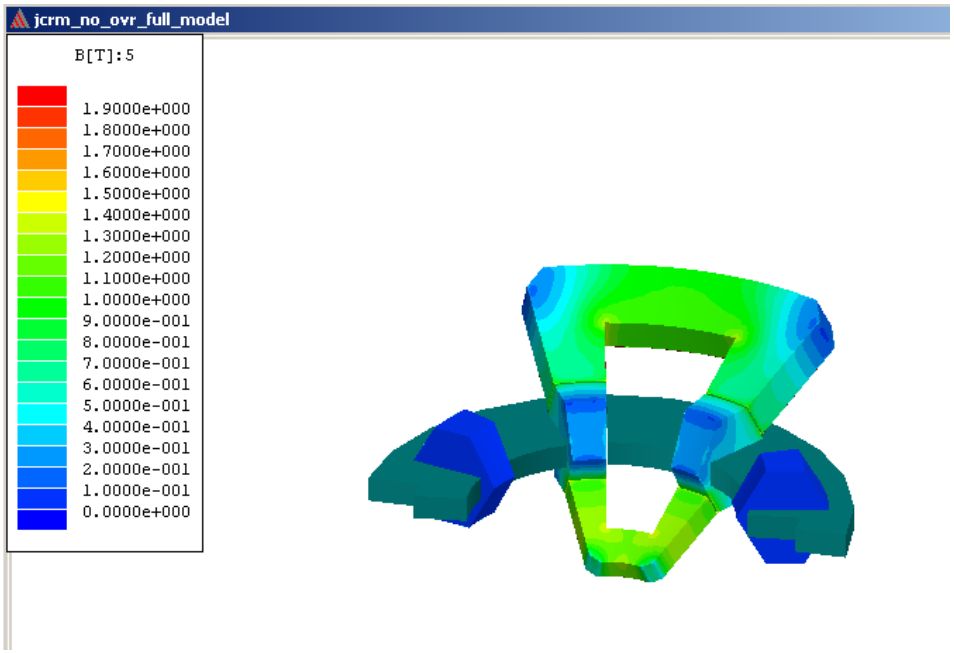

Figure 5.6: Aligned PhaseA with Chuck in Higher Saturation

path. This uneven saturation means that one chuck (of a chuck set) is in saturation while its complementary chuck may not be. In addition, the paths through the rotor are not perfectly symmetric. For a three phase scenario, Phases A and C will have a longer path while Phase B will have a slightly shorter path. Their paths will be longer because the rotor tooth has been slightly elongated to allow for the tooth to be fixed to the rotor hub. In a practical sense, non-uniform flux linkages will cause the motor controller to work harder, having to account for some stronger and some weaker phases. This early saturation of one chuck in a chuck set was verified by the FEA software Ansoft Maxwell3D. Figure 5.6 shows the smaller chuck to be in higher saturation than the larger chuck.

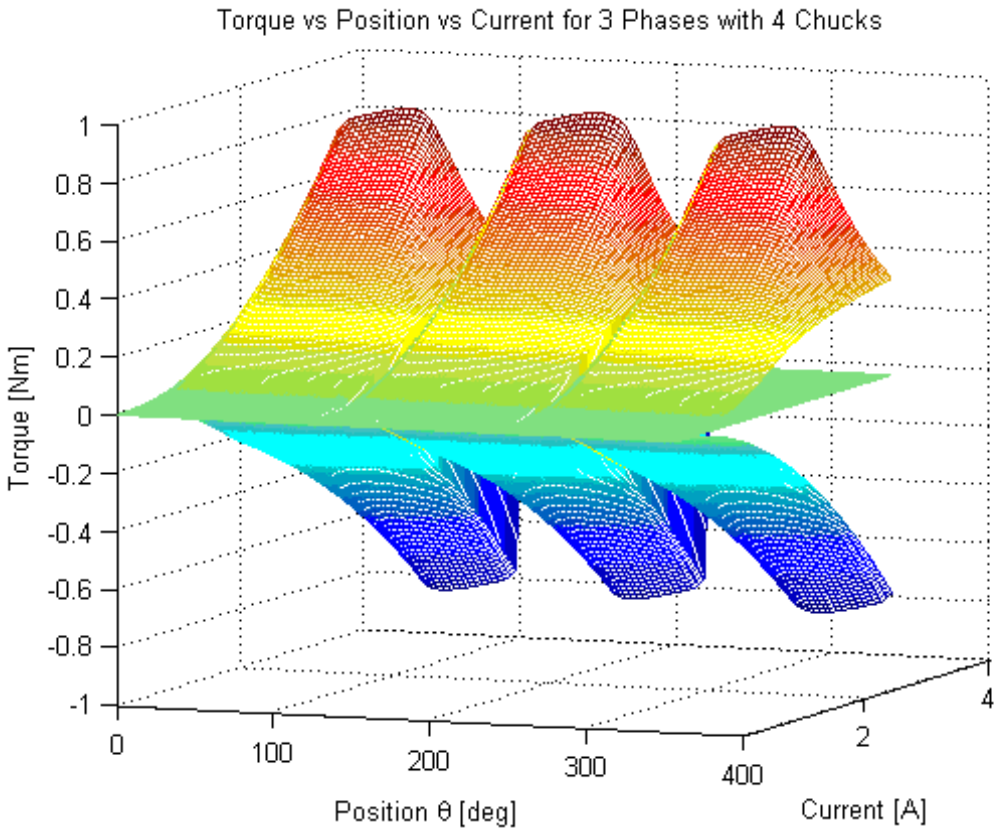

Figure 5.7: Torque for 3-Phases at 3.5A with 4 Chucks and Non-Overlapped

From this flux linkage plot, Figure 5.5, the torque may now be computed, as given in Equation 2.4, and is shown in Figure 5.7.

This torque is perhaps easier to understand from a 2D sense, which is shown in Figure 5.8. Each phase torque, shown in different colors, grows as the current and overlapping area grows. As the area peaks and begins to decline, the torque quickly reverses direction, thus the extreme change in torque direction. The various contours of each phase represent incremental current changes with the top most contour at 3.5A. Phase B, shown in black, shows strong agreement between the analytical and

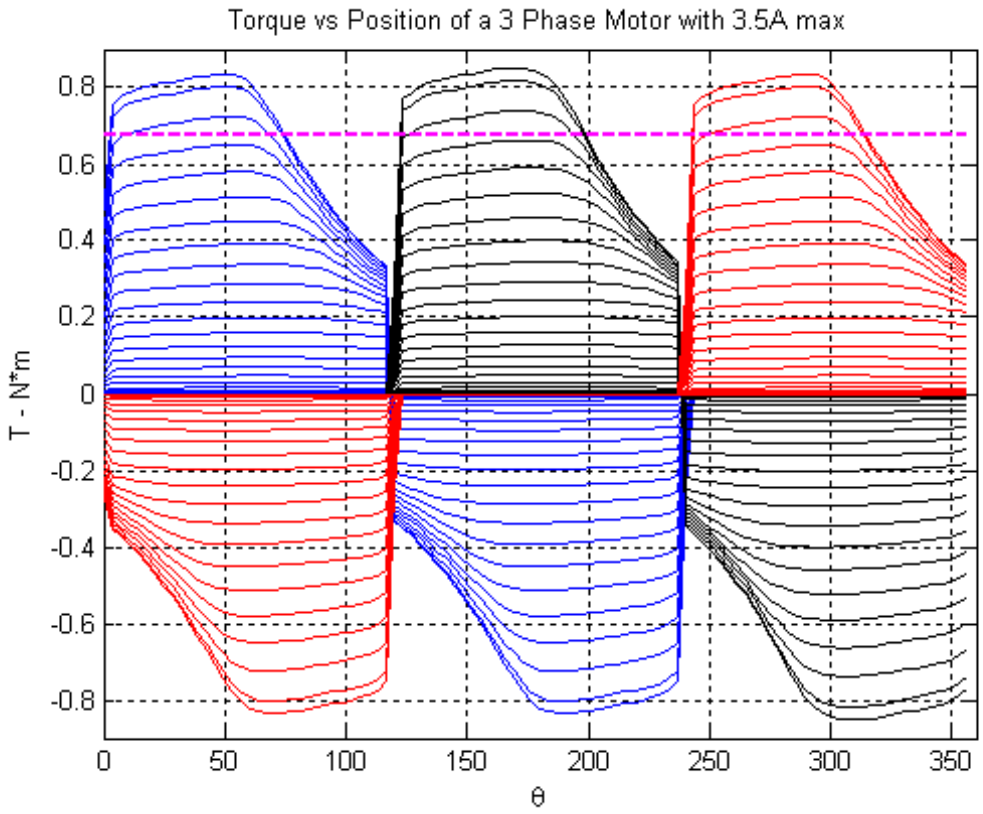

Figure 5.8: Torque Curves for Incremental Current Changes

FE results while Phase A and Phase C show lesser degree of agreement. The close agreement of Phase B is due to its unity face ratio, meaning the cross sectional area from one chuck to its complement does not change. While Phase B has a unity face ratio, phases A and C have a face ratio of 0.71 for this particular configuration. This reduction in cross sectional area is visible in Figure 5.8. Both plots also show the average torque of 0.69Nm in bold.

Notice in Figure 5.9 that the FEA plots of Phase A and C do not match that of Phase B. This is due to the early saturation of the smaller chuck of Phases A and C

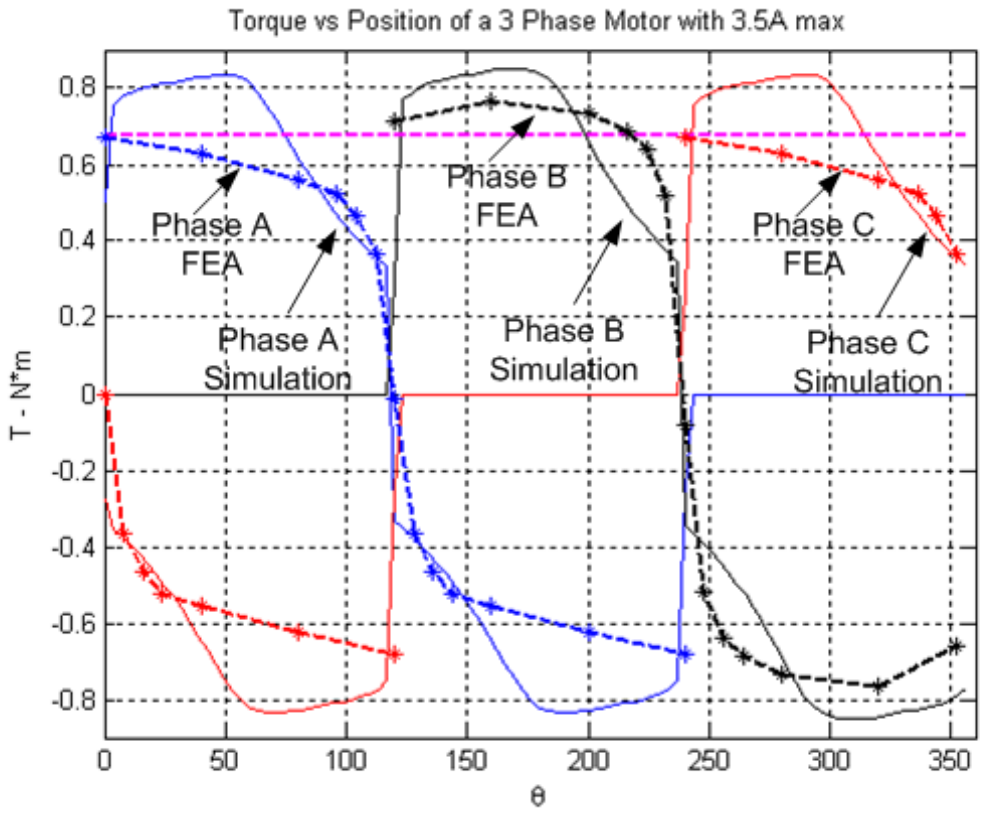

Figure 5.9: Comparison of Simulation to FEA at 3.5A

which have a smaller cross sectional area, as mentioned earlier. Also notice how the peak FEA torque of Phase B is greater than that of Phase A or C, resulting for the same reasons that lead to the simulation plot also having a higher torque value for Phase B, namely a unity face ratio.

Notice also that the FEA and simulation curves do not have the same shape although they do have close magnitude agreement. The differences between the FEA and simulation torque plots are due to the flux paths listed in Chapter 4 and the FEA flux paths. For Phases A and C the effects of saturation occur earlier in rotation than

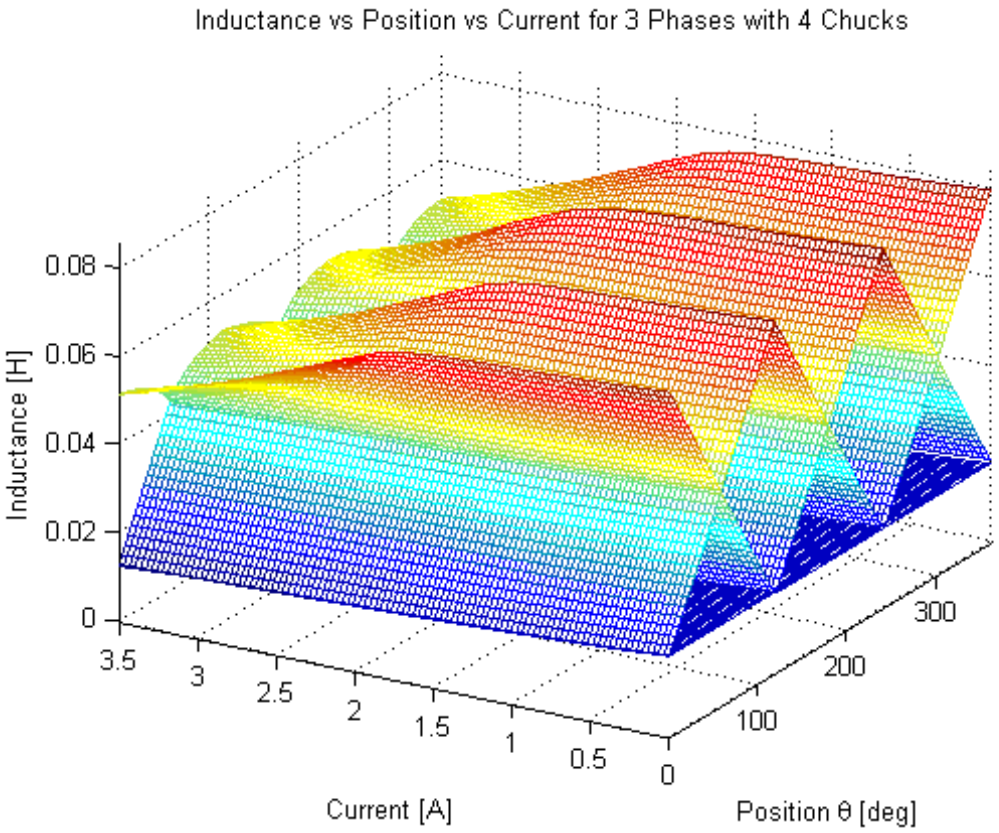

Figure 5.10: Inductance for 3-Phases at 3.5A with 4 Chucks and Non-Overlapped

predicted by the simulation but match during alignment. For Phase B, the simulation and FEA have early agreement but do not match as predicted by the simulation as alignment of the rotor and stator teeth peak.

The computed inductance for this motor is shown in Figure 5.10. From the figure notice that the inductance starts out higher than at maximum current. This is due to the reluctance being high initially, then tapering off as current increases and as saturation occurs, which accounts for the additional dip at currents above 2.5A.

During the torque computation from FEA, a force analysis has was also performed

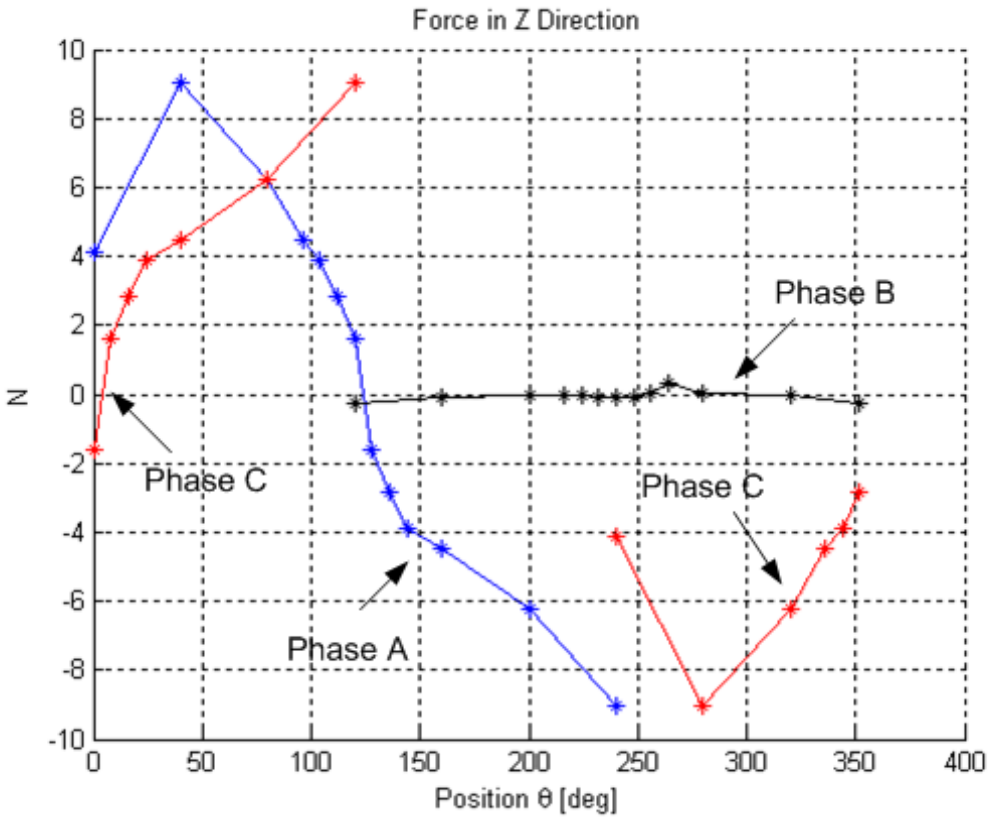

Figure 5.11: FEA Computed Forces Along Z-Axis

to help gage the mechanical loads that will arise upon the JCRM during operation. In particular, the loading along the z-axis (along motor shaft) is of interest as the JCRM topology will produce forces along this axis unlike traditional SR motors which produce mainly radial forces. Figure 5.11 shows these forces as computed by FEA. As expected Phase B has relatively little z-axis force, while Phases A and C have significantly more. This axial force will need to be addressed and compensated for prior to construction. If left unattended, premature mechanical failure and excessive audible noise may occur.

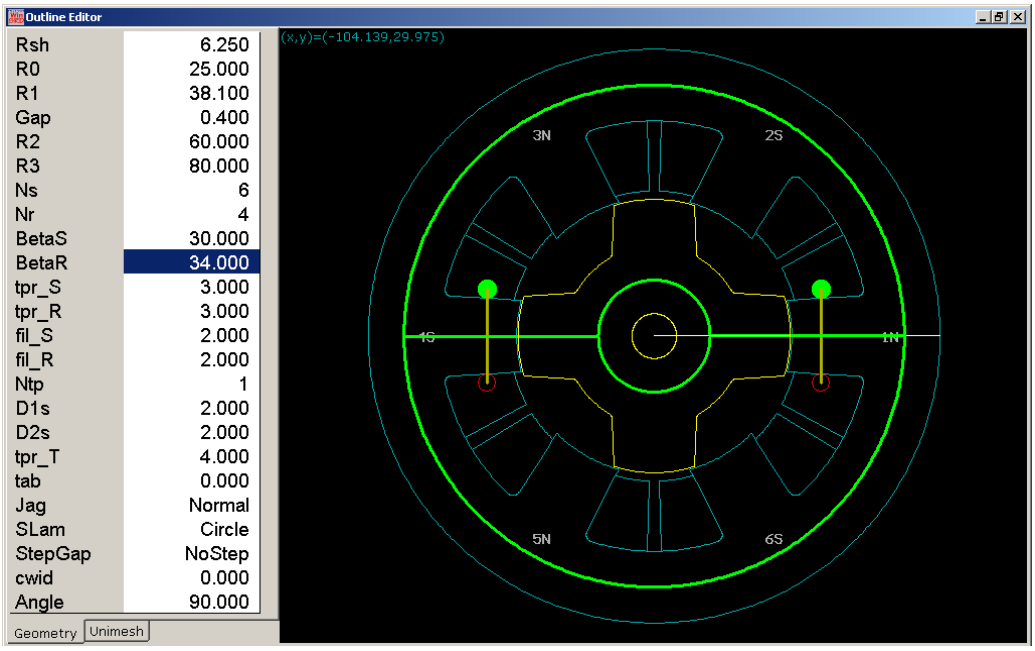

Figure 5.12: Outline of Resulting SR Motor Using SPEED

5.1 SPEED Comparison

In a further effort to gauge the design effectiveness and value, a traditional SRM has been analyzed with the commercially available motor design software *SPEED* from the University of Glasgow, UK [10]. The traditional SRM has been analyzed based upon a volume, phase number, current rating and wire size equal to the preceding JCRM design. The resulting traditional SRM created by SPEED is shown in Figure 5.12.

Utilizing this motor with equivalent parameters, the dynamic outputs of the motor can be obtained based upon internal software routines. Figure 5.13 shows the resulting current waveforms generated by SPEED. Notice the current ripple which is generated

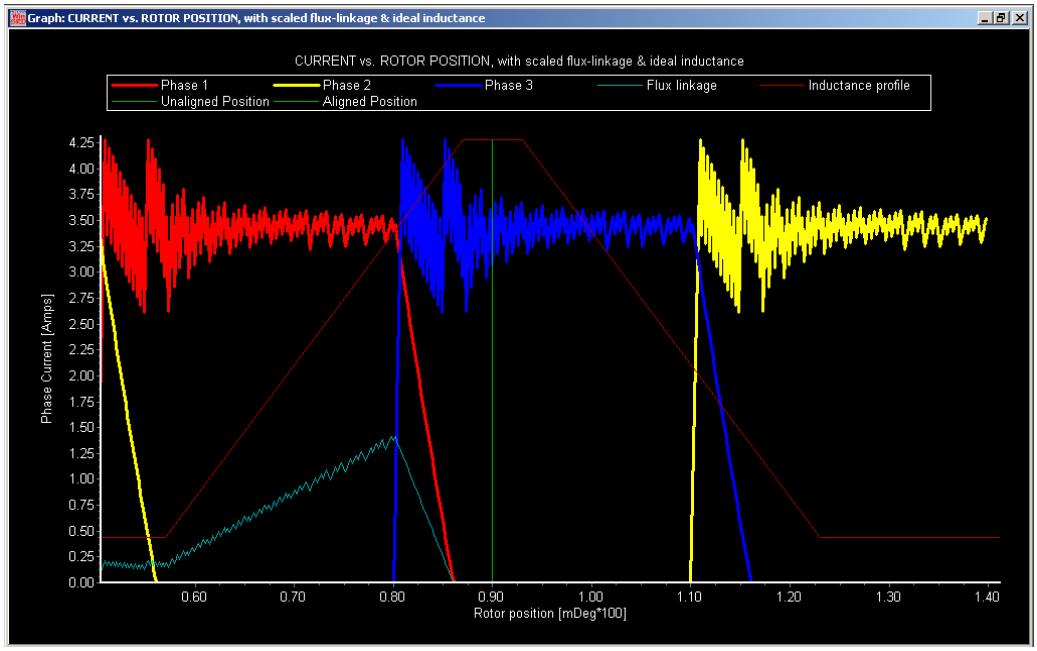

Figure 5.13: Currents for SPEED SR Motor

by SPEED as it tries to mimic an actual motor controller and limit the current to the predefined value of 3.5A.

The magnetization curves for the motor have also been generated via the SPEED software algorithm and are shown in Figures 5.14 and 5.15.

As done previously with the JCRM, the torque may now be computed from these magnetization curves and is shown in Figure 5.16. Notice that the torque has a large ripple at its aligned values corresponding to the current ripple mentioned previously.

The green horizontal line gives the average torque for the motor to be 0.29Nm. It is of great interest to note that this average value is less than that of the JCRM although the peak torque for the SRM is about that of the JCRM. The reason why

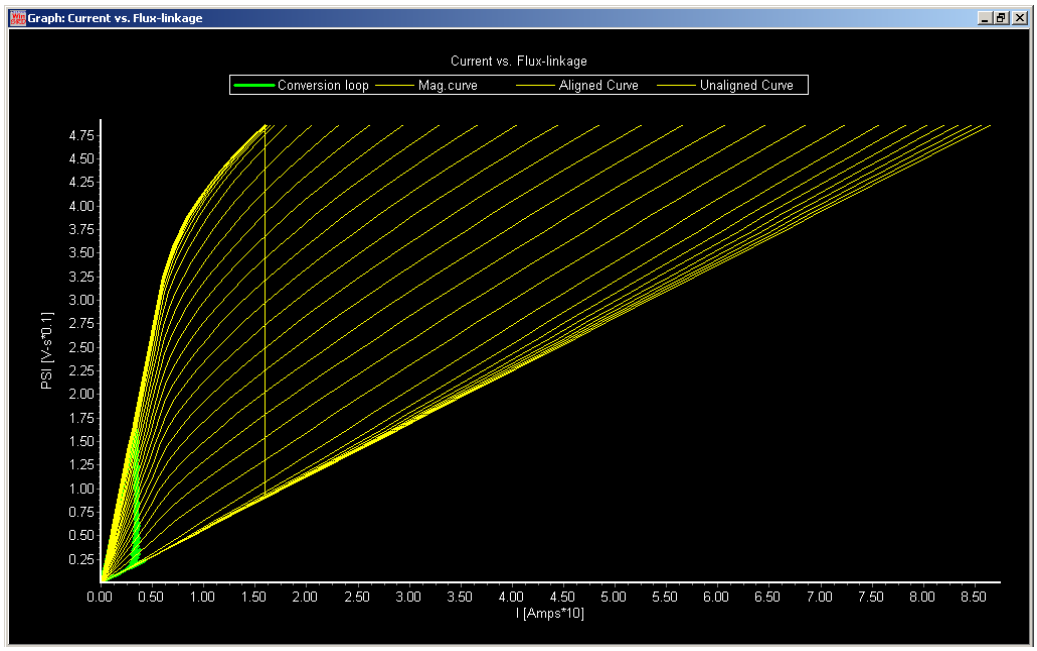

Figure 5.14: Flux Linkages for SPEED SR Motor

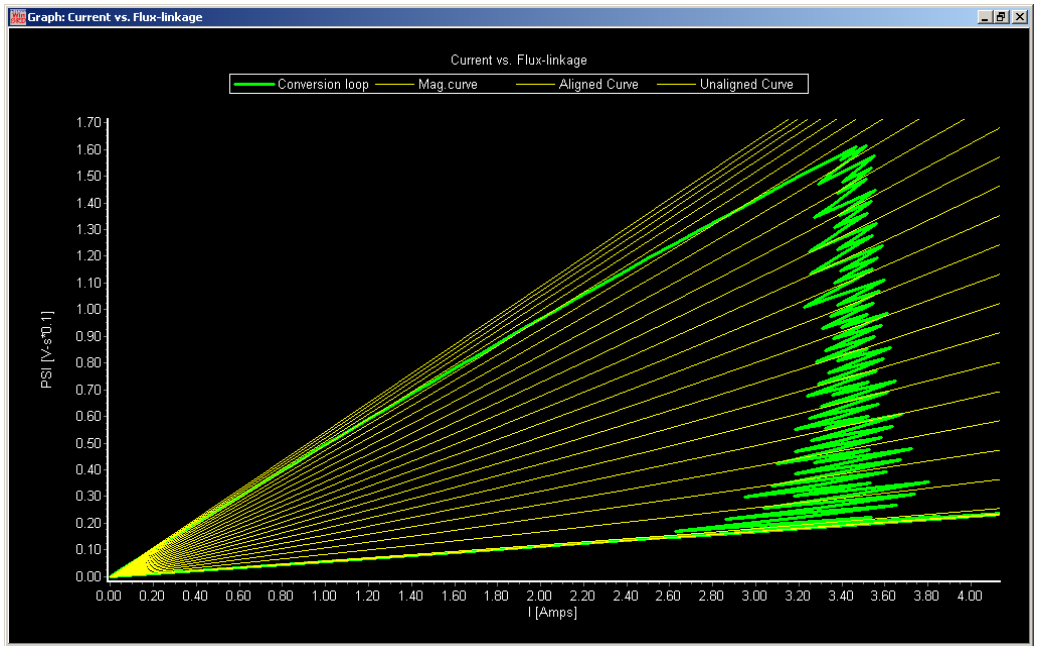

Figure 5.15: Zoom of Flux Linkage Curves for SPEED SR Motor

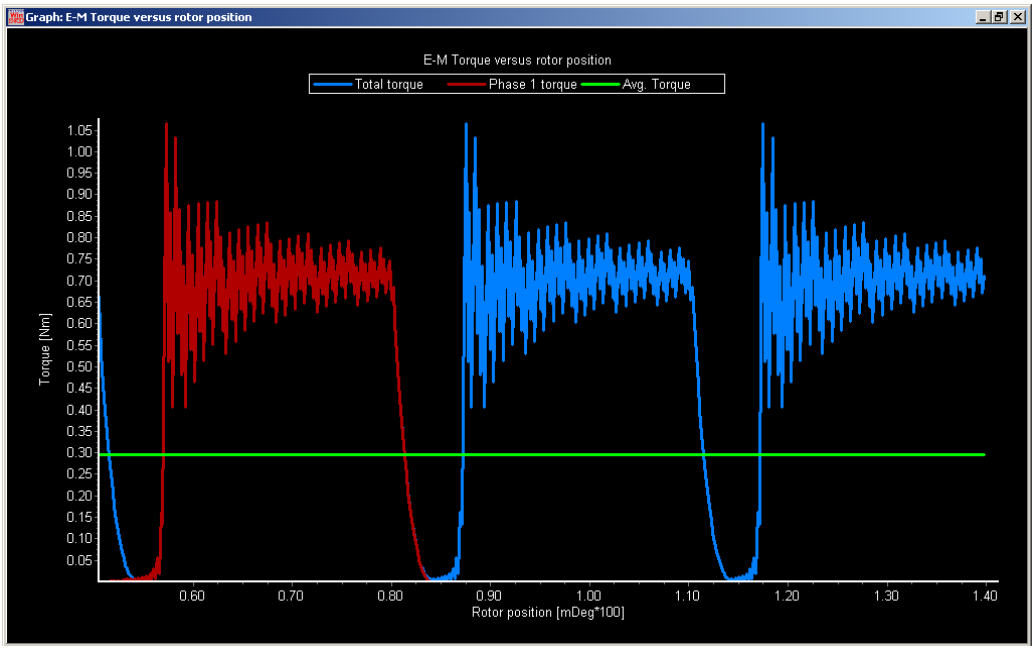

Figure 5.16: Torque vs Position for SPEED SR Motor

the traditional SRM has a lower average torque than the JCRM relates back to the fundamental design of the motors. In brief, the JCRM motor has less torque ripple thus a higher average torque. The reason for this lower torque ripple is due to the JCRM's ability to overlap the next phase without producing negative torque. As seen in Figure 5.12, the unaligned rotor teeth slightly overlap the stator teeth of two phases. As one of these phases begins to engage the other phase briefly shorts the flux path until the rotor has rotated through some angle whereby the path of least reluctance no longer includes the shorting stator tooth. In contrast, the JCRM does not suffer from this issue of flux shorting as the stator teeth and chucks reside in a transverse plane and the path of least resistance is through the rotor tooth. As seen

in Figure 5.12 the length of the shorting flux path is nearly equal to the path through the rotor yoke. This event does not occur in the JCRM as the path through the rotor tooth is much shorter than the path through an unaligned chuck.

It is also worth noting that for the two motors, the electrical rotation of the JCRM is equivalent to 45° mechanical degrees while the rotation of the SRM is equivalent to 90° mechanical degrees. This is important as it will cause the motor controller to cycle twice as often for equivalent shaft rotation thus require higher power ratings for the controller hardware and double the switching losses. This increase in cycle will also limit the maximum speed of the JCRM to a value less than the traditional SR motor.

5.2 Conclusion

This chapter has given the overall relations between the various elements of the new JCRM topology. These relations have been used to virtually construct a motor for initial parameterization. The motor has been simulated, and the results compared to FE analysis to gauge the value of the simulation, which has resulted in a favorable comparison. In addition, the design has been compared to a traditional SRM giving a rough estimation of how the JCRM compares to the traditional design.

Chapter 6

Conclusion

A new motor topology, intended for industrial application, has been explained and detailed. This topology, the Johnson-Currie Reluctance Motor, has features that are unique and of value to industry. The new motor topology introduced numerous new concepts such as stator chuck and chuck arrangements and eliminates several traditional ones such as the rotor and stator yokes. The motor produces flux linkages in three dimensions unlike any traditional motor style. In moving the flux producing coils out of the plane of rotation they are now accessible for removal and replacement should they fail, thus eliminating the requirement to replace the entire motor.

Moving the flux paths to three dimensions has given rise to several new construction possibilities. The topology no longer requires that the rotor, other than the rotor teeth, be constructed of permeable material. The rotor hub, used to hold fixed the rotor teeth, could be constructed of a high grade plastic or low grade aluminum,

whatever the application will allow. As the windings are no longer directly integrated into the stator, the motor's housing, like the rotor hub, may also be constructed of materials chosen for reasons other than their permeability. These material choices are a mass production cost reduction feature and of significant value to industry.

The design and analysis of the JCRM topology is more involved than a traditional style SRM which the JCRM is roughly based upon. While the technique for analysis of the JCRM is similar to that of the traditional SR motor, analysis of a single phase is not sufficient as the flux paths are no longer identical, a result of the complex geometry and a drawback of the new topology.

A three-inch diameter, four-chuck, three-phase JCRM with a maximum current of 3.5A has been analyzed for the non-overlapped design. The results from this analysis has shown close comparison to FEA results although additional work on defining flux paths is necessary for improved correlation. In addition, the results have been also been compared against a traditional SR motor. This comparison has shown that the average torque for the JCRM is higher than that of the traditional SRM due to a reduction in torque ripple.

The analysis presented in Chapters 4 and 5 assumed a lossless motor. Additional analysis of the JCRM motor which account for losses and further mechanical vibration analysis are necessary prior to building a prototype. This vibrational analysis is necessary as the forces that produce torque are no longer in the plane of rotation thus stress upon the rotor hub and shaft may induce failure upon these elements

earlier than with traditional SRMs. While vibrational issues exist, a motor that is inexpensive and repairable in place, such as the JCRM, is of interest to industry and thus worthy of continued research.

Future work necessary for the JCRM prior to construction includes the vibration and loss analysis as mentioned. In addition, a control method and motor drive scheme must be designed. This thesis has also presened several variations for the topology, overlapped and non-overlapped as well as coupled and looped. These topological variations need to be analyzed also to gain the complete picture of the JCRM.

Bibliography

Bibliography

1. "Motors and Generators: 2003", U.S. Department of Commerce Economics and Statistics Administration; November 2004, Table 2.

2. Timothy C. Moore and Amory B. Lovins,"Vehicle Design Strategies to Meet and Exceed PNGV Goals", The Hypercar Center Rocky Mountain Institue, pg19.

3. Amin Bahram, *"Variable Reluctance Machines - Analysis Design and Control"*, © 2003.

4. Dr. Duane Hanselman, *"Brushless Permanet Magnet Motor Design, Second Edition"*, The Writers' Collective, © 2003.

5. R. Krishnan, *"Switched Reluctance Motor Drives: Modeling Simulation, Analysis, Design and Applications"*, CRC Press, © 2001.

6. Arthur V. Radun, "Design Considerations for the Switched Reluctance Motor", *IEEE Transactions on Industry Applications*, Vol. 31, No 5, Pages: 1079 - 1087, September/October 1995.

7. M.N. Anwar, Iqbal Husain, Arthur V. Radun, "A Comprehensive Design Methodology for Switched Reluctance Machines", *IEEE Transactions on Industry Applications*, Vol. 37, No 6, Pages: 1684 - 1692, November/December 2001.

8. Vladan Vujicic, Slobodan N. Vukosavic, "A Simple Nonlinear Model of the Switched Reluctance Motor", *IEEE Transactions on Energy Conversion*, Vol 15, No 4, Pages: 395 - 400 December 2000.

9. T. J. Miller,*"Switched Reluctance Motors and their Control"*, Magna Physics Publishing and Clarendon Press-Oxford, 1993.

Vita

Weston Clute Johnson was born September 6, 1973 in Richmond, VA. He received his bachelors degree in electrical engineering in 1998 from Mercer University in Macon, GA. He joined Technicon Engineering, also of Macon, GA after his graduation from Mercer where he worked as an automation and controls engineer designing electrical systems for prototype industrial machinery. While at Technicon he worked with Mr. Richard Currie where the two conceived of the new motor topology described in this thesis. Weston will begin the Ph.D. program at the University of Kentucky, Lexington in August, 2005 for additional training and specialization in electrical machinery and design.